Author/s:
Kong, IY;Rimes, JS;Light, A;Todorovski, I;Jones, S;Morand, E;Knight, DA;Bergman, YE;Hogg, SJ;Falk, H;Monahan, BJ;Stupple, PA;Street, IP;Heinzel, S;Bouillet, P;Johnstone, RW;Hodgkin, PD;Vervoort, SJ;Hawkins, ED

Title:
Temporal Analysis of Brd4 Displacement in the Control of B Cell Survival, Proliferation, and Differentiation

Date:
2020-10-20

Citation:
Kong, I. Y., Rimes, J. S., Light, A., Todorovski, I., Jones, S., Morand, E., Knight, D. A., Bergman, Y. E., Hogg, S. J., Falk, H., Monahan, B. J., Stupple, P. A., Street, I. P., Heinzel, S., Bouillet, P., Johnstone, R. W., Hodgkin, P. D., Vervoort, S. J. & Hawkins, E. D. (2020). Temporal Analysis of Brd4 Displacement in the Control of B Cell Survival, Proliferation, and Differentiation. Cell Reports, 33 (3), https://doi.org/10.1016/j.celrep.2020.108290.

Persistent Link:
https://hdl.handle.net/11343/252630

Cell Reports

Article

Temporal Analysis of Brd4 Displacement in the Control of B Cell Survival, Proliferation, and Differentiation

Graphical Abstract

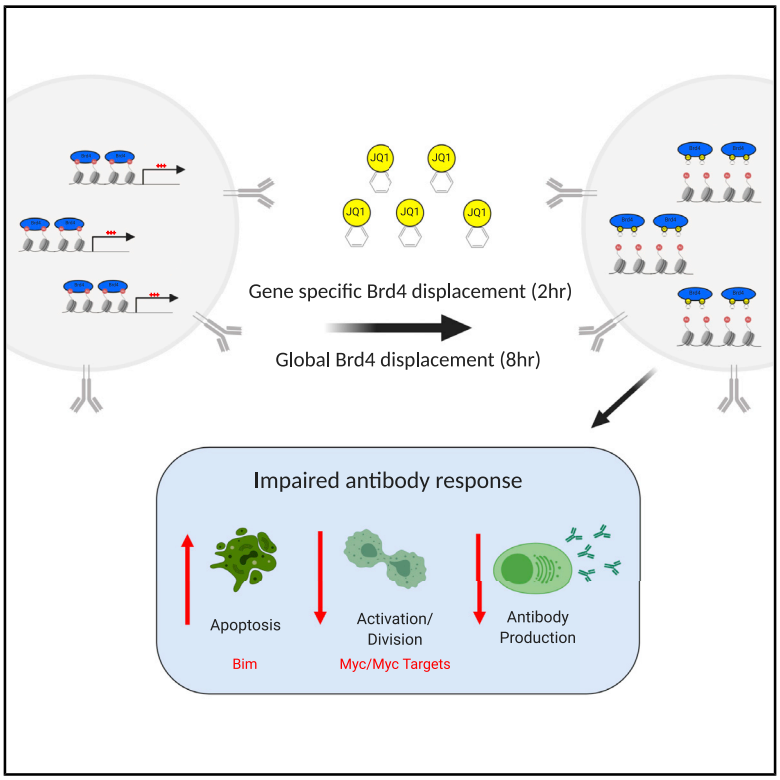

Highlights

- JQ1 affects B cell survival, proliferation, and as a consequence, antibody production
- Apoptosis induced by JQ1 is solely attributed to pro-apoptotic protein Bim
- JQ1 treatment causes temporal changes in Brd4 displacement
- Effects of JQ1 on B cell proliferation and survival are independently regulated

Authors

Isabella Y. Kong, Joel S. Rimes, Amanda Light, ..., Philip D. Hodgkin, Stephin J. Vervoort, Edwin D. Hawkins

Correspondence

stephin.vervoort@petermac.org (S.J.V.), hawkins.e@wehi.edu.au (E.D.H.)

In Brief

Kong et al. show that JQ1 affects multiple aspects of B cell function, including survival, proliferation, and as a consequence, antibody production. JQ1-induced apoptosis is solely attributed to the pro-apoptotic protein Bim. JQ1 treatment drives temporal changes in Brd4 displacement, resulting in a specific transcriptional profile.

Kong et al., 2020, Cell Reports *33*, 108290
October 20, 2020
https://doi.org/10.1016/j.celrep.2020.108290

CellPress

Cell Reports

CellPress
OPEN ACCESS

Article

Temporal Analysis of Brd4 Displacement in the Control of B Cell Survival, Proliferation, and Differentiation

Isabella Y. Kong,[1,2,8] Joel S. Rimes,[1,2,8] Amanda Light,[1,2] Izabela Todorovski,[3,4] Sarah Jones,[5] Eric Morand,[5] Deborah A. Knight,[3,4] Ylva E. Bergman,[6,7] Simon J. Hogg,[3,4] Hendrik Falk,[1,6] Brendon J. Monahan,[1,6] Paul A. Stupple,[6,7] Ian P. Street,[1,6] Susanne Heinzel,[1,2] Philippe Bouillet,[1,2] Ricky W. Johnstone,[3,4] Philip D. Hodgkin,[1,2] Stephin J. Vervoort,[3,4,8,*] and Edwin D. Hawkins[1,2,8,9,*]

[1]Walter and Eliza Hall Institute of Medical Research, The University of Melbourne, 1G Royal Parade, Parkville, VIC 3052, Australia
[2]Department of Medical Biology, The University of Melbourne, Parkville, VIC 3010, Australia
[3]Cancer Therapeutics and Cancer Immunology Program, Peter MacCallum Cancer Centre, Melbourne, VIC, Australia
[4]Sir Peter MacCallum Department of Oncology, The University of Melbourne, Melbourne, VIC, Australia
[5]Centre for Inflammatory Diseases, School of Clinical Sciences, Monash University, Parkville, VIC 3052, Australia
[6]Cancer Therapeutics CRC (CTx), Melbourne, VIC 3000, Australia
[7]Medicinal Chemistry, Monash Institute of Pharmaceutical Sciences, Monash University, Parkville, VIC 3052, Australia
[8]These authors contributed equally to this work
[9]Lead Contact
*Correspondence: stephin.vervoort@petermac.org (S.J.V.), hawkins.e@wehi.edu.au (E.D.H.)
https://doi.org/10.1016/j.celrep.2020.108290

SUMMARY

JQ1 is a BET-bromodomain inhibitor that has immunomodulatory effects. However, the precise molecular mechanism that JQ1 targets to elicit changes in antibody production is not understood. Our results show that JQ1 induces apoptosis, reduces cell proliferation, and as a consequence, inhibits antibody-secreting cell differentiation. ChIP-sequencing reveals a selective displacement of Brd4 in response to acute JQ1 treatment (<2 h), resulting in specific transcriptional repression. After 8 h, subsequent alterations in gene expression arise as a result of the global loss of Brd4 occupancy. We demonstrate that apoptosis induced by JQ1 is solely attributed to the pro-apoptotic protein Bim (*Bcl2l11*). Conversely, cell-cycle regulation by JQ1 is associated with multiple Myc-associated gene targets. Our results demonstrate that JQ1 drives temporal changes in Brd4 displacement that results in a specific transcriptional profile that directly affects B cell survival and proliferation to modulate the humoral immune response.

INTRODUCTION

BET proteins feature two conserved N-terminal bromodomains that interact with acetylated lysine residues on histones (and other proteins), resulting in the localization of BET proteins such as BRD4 to hyperacetylated chromatin locations (Patel et al., 2013). BRD4 exerts its effect by interacting with positive transcription elongation factor complex (P-TEFb) to promote transcription elongation of RNA polymerase II (Pol II) by directly phosphorylating the Pol II C-terminal domain as well as the negative elongation factor (NELF) and 5,6-dichloro-1-β-D-ribofuranosylbenzimidazole (DRB) sensitivity-inducing factor (DSIF) (Zuber et al., 2011). Thus, BRD4 can be characterized as a general transcriptional regulator. Previously, BET bromodomain proteins were associated with immune cell processes, including virus latency, post-mitotic memory, and inflammation, as well as the development of neoplasms from immune lineages such as hematopoeitic malignancies (Gilan et al., 2016; Díaz et al., 2017; Mertz et al., 2011). In line with these findings, BRD4 has been linked to c-MYC-dependent transcription (Heinzel et al., 2017), a molecular mechanism intimately linked to the expansion of B cells in both protective (Adams et al., 1985) and pathogenic settings (Filippakopoulos et al., 2010). Thus, there is strong interest in understanding the molecular mechanisms of targeting BET proteins in the context of therapeutic intervention, cancer, and modulation of protective immune responses.

JQ1 is a potent inhibitor of the BET family of bromodomain proteins. JQ1 binds competitively to the histone acetyl-lysine-bromodomain complex and displaces the complex from the chromatin (Stathis and Bertoni, 2018). This prevents the recruitment of key core transcriptional regulators and consequently blocks transcription. JQ1 has been shown to induce cytotoxicity in a variety of malignancies (reviewed by Delmore et al., 2011), including multiple myeloma (Delmore et al., 2011), by inhibiting tumor growth and survival, causing cell-cycle arrest, and inhibiting differentiation. While the function of JQ1 in the context of many immune cell contexts has been investigated, the underlying mechanisms are still unclear. For example, numerous studies have suggested that JQ1 acts by modulating

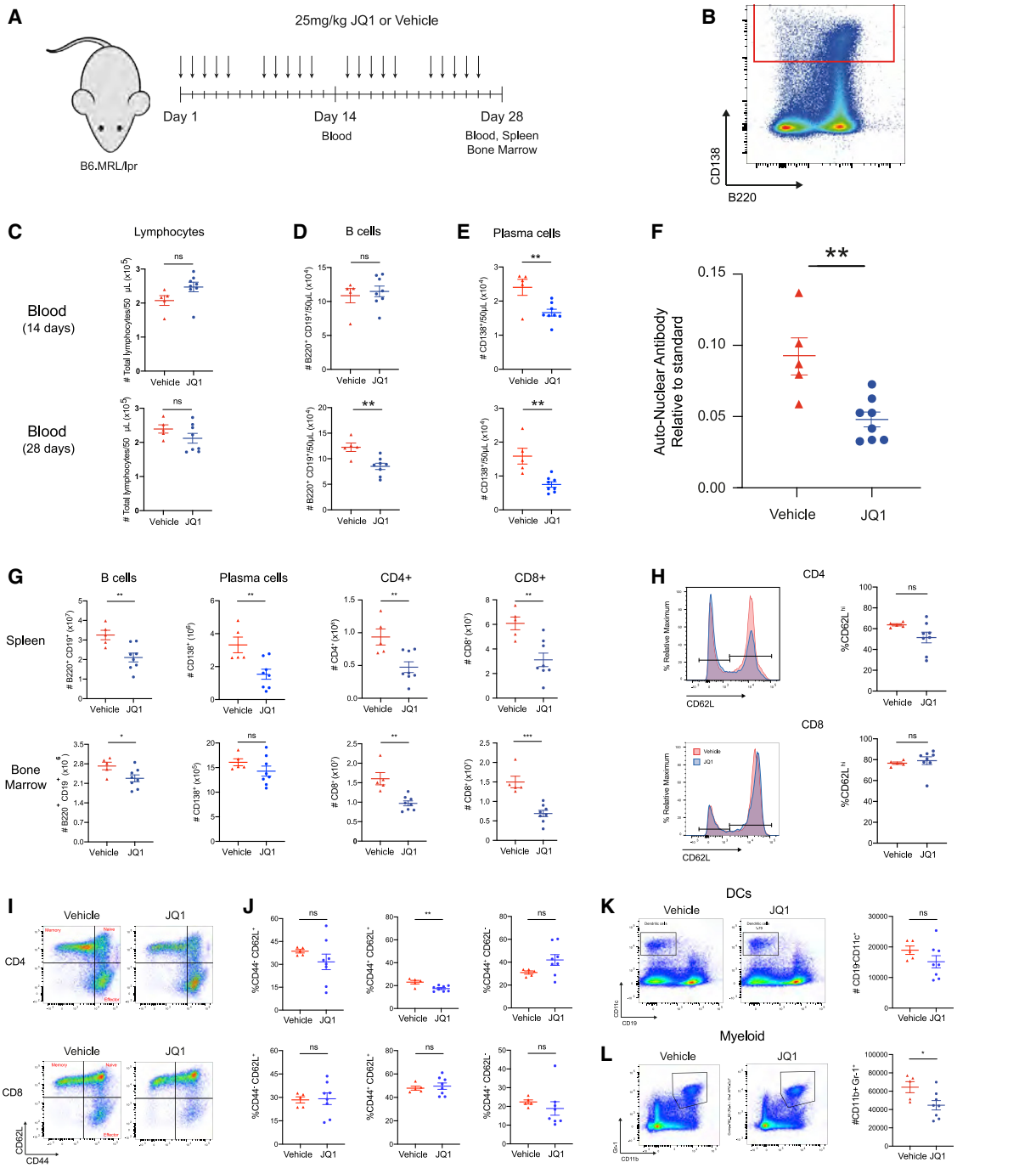

Figure 1. The Effect of JQ1 on Immune Cell Subsets in MRL/lpr Autoimmune-Prone Mice

(A) Male MRL/lpr mice 5–8 weeks of age were treated with either 25 mg/kg JQ1 or vehicle for 4 weeks. Blood samples were collected 14 days post-JQ1 treatment. Endpoint analysis was performed on blood, spleen, and bone marrow. Cell numbers were quantified relative to a known number of calibration beads.

(B) Example gating strategy for plasma cells ($CD138^+$).

(C–E) Total lymphocytes (C), B cells (D) and plasma cells (E) in blood quantified relative to a known number of calibration beads.

(F) Pooled auto-nuclear antibodies (ANAs) in the serum of mice at the endpoint.

(G) Total B cells, plasma cells, $CD4^+$, and $CD8^+$ T cells in spleen or bone marrow quantified relative to a known number of calibration beads.

(H) Proportion of $CD62L^+$ $CD4^+$ and $CD8^+$ T cells.

(I) Gating strategy for CD44 and CD62L for CD4 and CD8 T cells.

(legend continued on next page)

MYC or MYC-dependent pathways (Hogg et al., 2017). However, contrasting reports illustrate that the efficacy of JQ1 is often unrelated to the downregulation of MYC, and this action alone is insufficient to drive cell-cycle arrest and inhibit survival (Hogg et al., 2017). BET bromodomain inhibitors have also been explored as immunomodulatory compounds, either to suppress pro-inflammatory signals in autoimmune diseases or to promote immune responses in the context of cancer (Kagoya et al., 2016; Peeters et al., 2015; Burnet, 1976). However, the functional outcomes of targeting BET proteins in the context of therapeutic intervention, cancer, and healthy immunity remain poorly understood.

Here, we have combined quantitative analyses at multiple levels from immune cell function to genomics to investigate the molecular consequences of the treatment of B cells with JQ1 and the underlying molecular processes related to the regulation of antibody responses. Clonal expansion of B cells is a complex process (Baell et al., 2018), and errors at checkpoints throughout this process can lead to the development of autoimmunity or B cell neoplasms. Thus, understanding the molecular processes that underpin these fate decisions and potential therapeutic interventions is paramount. As B cell subsets are sensitive to compounds that target epigenetic machinery in a gene-dependent and compound-dependent manner (Waibel et al., 2015; Xu et al., 2016), we used the protective antibody response as a system to investigate the molecular mechanisms of JQ (Hawkins et al., 2007b).

To dissect these effects in greater resolution, we applied mathematical methods based on the Cyton model (Hawkins et al., 2007b). In this model, a small number of independent quantifiable parameters are used to describe B cell and T cell proliferation, survival, and differentiation following stimulation (Hawkins et al., 2007a, 2007b, 2013a; Duffy et al., 2012; Turner et al., 2008; Waibel et al., 2015; Dowling et al., 2018; Markham et al., 2010; Rizzitelli et al., 2006). This quantitative framework enables the effect of different compounds on isolated lymphocyte functions to be examined in detail (Watanabe-Fukunaga et al., 1992). By pairing this approach with genomic studies, we sought to gain insights into the gene targets of JQ1 and the molecular mechanisms that control lymphocyte responses. We show that JQ1 directly affects multiple components of the antibody response, including the induction of apoptosis and reduced proliferation and inhibition of effector cell differentiation. We demonstrate that the reduction of antibody production occurs indirectly through the inhibition of cell division, rather than modifying the differentiation program itself. Genome-wide characterization of the JQ1 response in stimulated B cells demonstrates that these phenotypic responses are the result of global Brd4 displacement, which drives a remarkably limited and specific transcriptional response exemplified by the exclusive dependency on the pro-apoptotic molecule Bim to induce apoptosis in stimulated B cells in response to JQ1.

RESULTS

JQ1 Treatment Causes Broad Immunosuppression *In Vivo*

To determine the effect of JQ1 on B cell subsets *in vivo*, we investigated its immunosuppressive effects in pre-clinical models of immune disorders linked to hyper-proliferative lymphocyte subsets and antibody-mediated disease. We used the B6.MRL/*lpr* mouse model, which carries the *lpr* mutation in Fas (CD95) and develops autoimmune pathology characterized by the systemic immune activation of multiple lymphocyte subsets and the accumulation of autonuclear antibodies (ANAs) reactive against multiple nuclear antigens, including DNA and histones, akin to those seen in patients with systemic lupus erythematosus (SLE) (Waibel et al., 2015). In addition, these B cell subsets are sensitive *in vivo* to therapeutic targeting with histone deacetylase inhibitor (HDACi) (Tyler et al., 2017). Groups of B6.MRL/*lpr* mice were treated with either 25 mg/kg JQ1 (5 days on, 2 days off) or vehicle for 28 days (Figure 1A). Blood was sampled at 2-week intervals for the 4-week treatment period to measure immune cell subset numbers by flow cytometry (Figures 1B–1E) and serum ANA levels (Figure 1F). Treatment with JQ1 was well tolerated, with steady weight gain observed throughout the treatment period (Figures S1A and S1B). While total cellularity of blood remained relatively unaffected at 14 and 28 days post-treatment (Figure 1C), we noted a gradual loss of B cells and plasma cells over the 4-week treatment window (Figure 1D and 1E). This led to a significant loss of circulating autoreactive plasma cell populations. At the end of the treatment period, we also measured numerous immune cell subsets in addition to B cells in the spleen and bone marrow. Consistent with time course measurements of peripheral blood, we observed a significant reduction in CD19/B220$^+$ B cells and CD138$^+$ plasma cells in the spleens of treated mice (Figure 1G). The effects of JQ1 on B cells and plasma cells were lesser in the bone marrow, a finding that is consistent with previous studies tracing the access of modified JQ1 derivatives across the bone marrow niche (Hawkins et al., 2013b). In addition, we noted significant reductions in CD4$^+$ and CD8$^+$ T cells in both the spleen and bone marrow (Figure 1G). We evaluated whether JQ1 specifically reduced naive or activated T cell subsets by comparing the proportion of L-selectin (CD62L)-expressing T cells remaining in the reduced viable population (Figure 1H). We observed no selection for naive (CD62L^{hi}) or activated (CD62L^{lo}) CD4$^+$ and CD8$^+$ T cells, suggesting that JQ1 did not target T cell populations in a specific manner in regard to populations identified solely on CD62L expression. We further expanded this analysis to include effector and memory T cells based on CD44 and CD62L expression (Figure 1I). We noted no significant difference in any CD4$^+$ or CD8$^+$ T cell population, with the exception of CD4$^+$CD44$^+$CD62L$^+$ naive cells that were reduced in JQ1-treated mice (untreated: mean 23.04%, SEM 1.54%; JQ1: 17.44%, SEM 0.85%; Figure 1J). Thus, although reduced in

(J) Proportion of naive (CD44$^-$ CD62L$^+$), central memory (CD44$^+$ CD62L$^+$), and effector (CD44$^+$ CD62L$^-$) for CD4$^+$ and CD8$^+$ T cells.
(K and L) Proportion and number of (K) dendritic cells (CD11c$^+$) and (L) myeloid cells (Gr-1$^+$ CD11b$^-$).
Vehicle, n = 5, JQ1 treated, n = 8. Error bars denote means ± SEMs. Significance differences were determined using 2-tailed unpaired Student's t tests. *p < 0.05, **p < 0.01, ***p < 0.001, and ****p < 0.0001.

number, the change in the distribution of T cell subsets was unremarkable, suggesting that the activation state did not affect the sensitivity to JQ1 treatment. In addition, we measured the number of dendritic cells and myeloid cells based on CD11c/CD19 (Figure 1K) and CD11b/Gr-1 expression, respectively (Figure 1L). Although both populations were slightly reduced in the spleens of JQ1-treated mice, a significant reduction was only noted in $CD11b^{+}Gr\text{-}1^{+}$ myeloid cells. B6.MRL/*lpr* mice develop cervical lymphadenopathy, which subsequently affects the breathing and general well-being of mice with advanced disease. We observed a profound reduction in the size and cellularity of cervical nodes following JQ1 treatment (Figure S1C). Thus, our results illustrate that JQ1 has a broad-spectrum systemic suppressive effect on immune cells, including the B cell and plasma cell lineages.

JQ1 Inhibits Antibody Production and Reduces B Cell Survival *In Vitro*

To interrogate the effect of JQ1 on B cell function in more detail, we performed a quantitative *in vitro* analysis of B cell responses and gene regulation. We investigated the effect of JQ1 on the T cell independent (TI) antibody response by measuring antibody levels in the supernatant following 4 days *in vitro* culture with lipopolysaccharide (LPS) (Deenick et al., 1999). JQ1 led to a dose-dependent reduction in the total levels of secreted immunoglobulin M (IgM) (Figure 2A). To determine the impact of LPS-stimulated class switching, we measured the proportion of cells that lost the expression of IgM per division (i.e., the collective commitment to all other Ig subtypes) and noted a significant decrease in the total proportion of IgM^{-} switched cells (Figures S1D and S1F) and switched cells per division (Figures S1E and S1F). Similarly, in the context of T-dependent stimulation with $\alpha CD40^{+}$IL-4, both the proportion of total $IgG1^{+}$ switched cells (Figures S1G and S1I) and isotype switching per division (Figures S1H and S1I) was reduced.

As antibody levels are the net product of B cell proliferation and differentiation (Hasbold et al., 2004; Hawkins et al., 2013b), we asked whether JQ1 directly targeted differentiation into antibody-secreting cells (ASCs) and production of secreted IgM, or alternatively, whether these changes in differentiation were linked to altered cell division and survival. We stimulated Cell Trace Violet (CTV)-labeled follicular B cells with LPS to induce a substantial traceable ASC population *in vitro* (Rathert et al., 2015) and measured the total proportion of $CD138^{+}$ cells. JQ1 significantly reduced the proportion of $CD138^{+}$ cells in culture (Figure 2B). When analyzed in relation to cell division, it was clear that the loss of ASC differentiation resulted from stalling the progression of B cells through division and therefore reduced division-dependent differentiation into $CD138^{+}$ cells (Figure 2C). This observation was confirmed when ASC were quantified relative to cell division. The effect of JQ1 on B cell differentiation was minimal, indicating that the reduction in total ASC differentiation was predominantly a result of impaired cell division (Figure 2D; Table S1) rather than changes in differentiation rates per division.

JQ1 has been reported to have multiple context-specific effects in certain tumor cell types, including induction of apoptosis (Xu et al., 2016; Fong et al., 2015; Hawkins et al., 2013b). Therefore, we measured the induction of cell death in LPS-activated B cells in response to JQ1. Small naive B cells were stimulated with LPS in varying concentrations of JQ1, and viability was measured after 48 h via uptake of propidium iodide (PI). In a similar fashion to antibody production and proliferation, treatment with JQ1 had a significant dose-dependent effect on cell viability (Figures 2E and 2F). These findings suggest that JQ1 affects the humoral immune response by targeting multiple components of the B cell response.

Quantifying the Effect of JQ1 Treatment on B Cell Responses *In Vitro*

To dissect the effect of JQ1 treatment on B cell function, we performed a quantitative analysis using the Cyton model, a probabilistic model of lymphocyte responses that provides a framework to perform non-biased quantitative analysis of division tracking data of viable lymphocytes *in vitro* (shown for B cells in response to titrated doses of JQ1 in Figure 3A), called "cohort analysis." This approach removes the effect of cell expansion of cells per division to allow the fate of original founding cells that are recruited into the antibody response to be measured. Using this approach, the cohort number over time enables changes in the cell survival to be measured (Figure 3B). In addition, measuring progression through division by calculating the mean division number of responding cells over time, accurate measurements of proliferation kinetics can be determined (Figure 3C). This includes the mean time for immune cell populations to initiate activation (mean time to first division), the division rate of activated cells, and the maximum number of cell divisions the population of cells undergo before quiescence (division destiny) (Figure 3C). By using this approach, we could fully describe the features of the B cell response to JQ1 treatment and link the underlying molecular effects to quantitative changes through extensive molecular profiling.

Small resting follicular B cells were purified from the spleens of C57BL/6 mice, labeled with the division tracking dye CTV, and the effects of JQ1 were measured in the context of TI stimulation. In addition to LPS, we also investigated the Toll-like receptor 9 (TLR-9) ligand CpG, which induces B cell activation in the absence of ASC differentiation and isotype switching. This allows the impact on cell division and survival independent of differentiation to be measured (Adams et al., 1985). Time course analysis was performed over 4 days in culture, and B cell numbers per division were quantified relative to a known number of calibration beads added to samples at the point of analysis by flow cytometry (Figure 3D). JQ1 had a broad range of effects on multiple components of the B cell response (Figures 3D–3F; Table S2). This included induction of cell death in both dividing and non-dividing B cell populations (as indicated by reduced cohort number over time; Figure 3E), consistent with earlier measurements of cell death in undivided B cells (Figure 2E). However, we also noted significant effects on B cell activation (time taken for B cells to progress through the first division) and the kinetics of proliferation (subsequent division times). This is reflected in graphical analysis by a reduced intercept with 1 on the y axis (indicating delays in entry to the first division), a reduced gradient of the cohort plot (delayed division rates/cell-cycle times), and reduced maximum division numbers (division destiny) (Figure 3F). These effects were consistent in both LPS and CpG

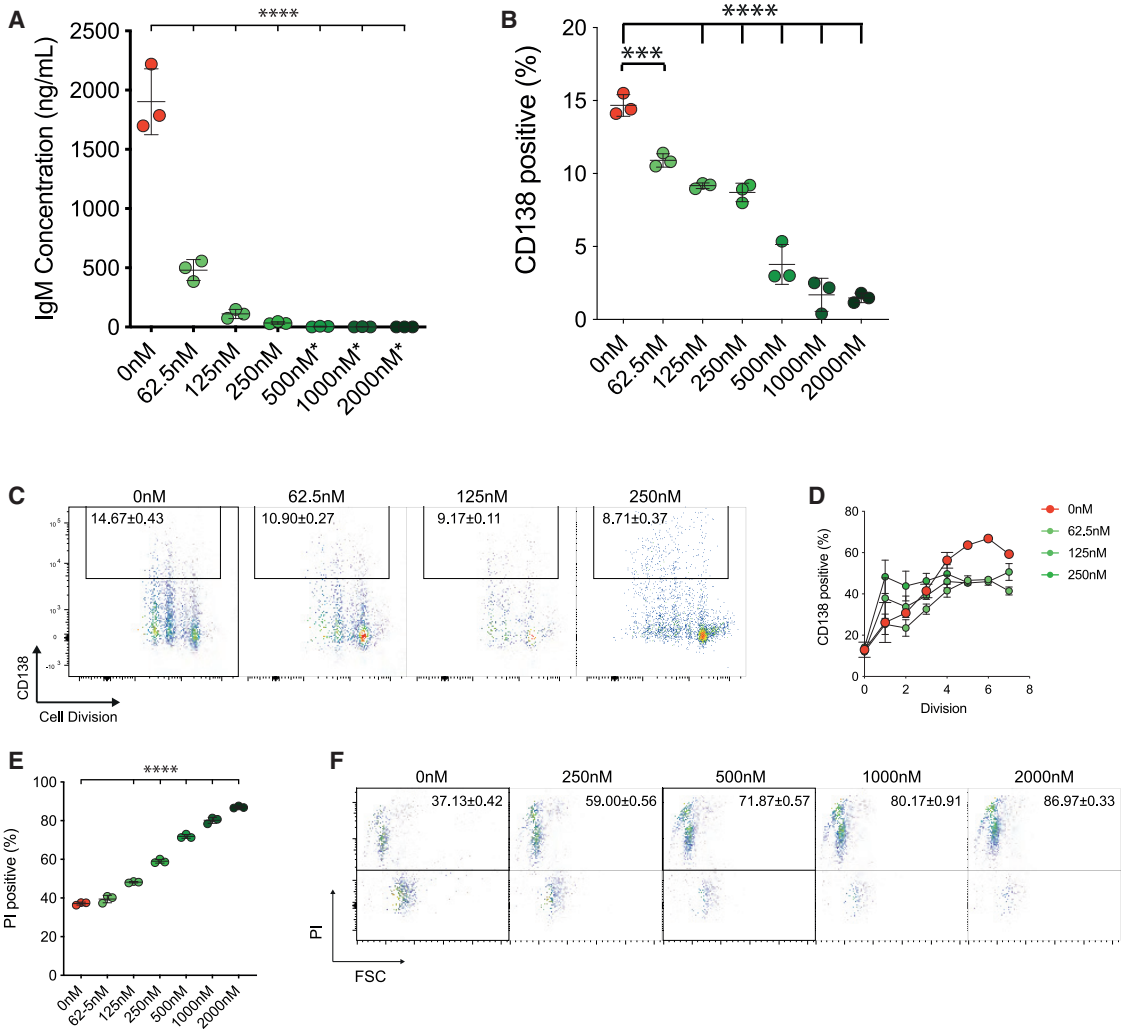

Figure 2. JQ1 Treatment Results in Reduction in Antibody Production, Isotype Switching, and Survival of B Cells *in vitro*

Purified CTV-labeled B cells were stimulated with LPS in the presence of indicated concentrations of JQ1.

(A) IgM production 4 days post-stimulation.

(B and C) Percentage of differentiated cells 4 days post-stimulation (B), and (C) representative plots are shown.

(D) Percentage of differentiated cells per division.

(E and F) Cell death resulting from JQ1 treatment at 48 h post-stimulation measured by propidium iodide staining (E), and (F) representative plots are shown.

The data in (C) and (F) are representative plots from triplicate samples. The data in (A)–(F) are means ± SEMs of triplicate samples. All of the data are representative from 3 independent experiments. All of the statistical tests were performed in comparison to untreated controls. Significance differences were determined using ANOVA Bonferroni corrections. **$p \leq 0.01$ and ****$p \leq 0.0001$.

stimulation. This indicates that JQ1 directly targets antibody responses by inducing apoptosis and inhibiting the activation and division progression of B cells (Figure 2).

JQ1 has been reported to exert its biological effects in hematopoietic lineage cells through the targeted downregulation of Myc, a key transcriptional pathway linked to the cell cycle and apoptosis (Zuber et al., 2011; Heinzel et al., 2017). As Myc levels have recently been described as a key component of a division "timer" that modulates the level of expansion of the antibody response (division destiny) (Muhar et al., 2018), we measured the effect of JQ1 treatment on Myc in the context of *in vitro* antibody responses (Figure 3G). We found significant dose-dependent downregulation of Myc by JQ1 (Figures 3H and 3I). Furthermore, when measured on a per-division basis, Myc downregulation was found to occur concomitantly as the progression of B cells through division was stalled (Figures 3I, S2A, and S2B). These results suggest that JQ1 inhibits B cell expansion and the antibody response by targeting the Myc pathway.

JQ1 Treatment in B Cells Induces Global Displacement of Brd4

On a molecular level, JQ1 mediates the displacement of BET bromodomain-containing proteins, thereby perturbing

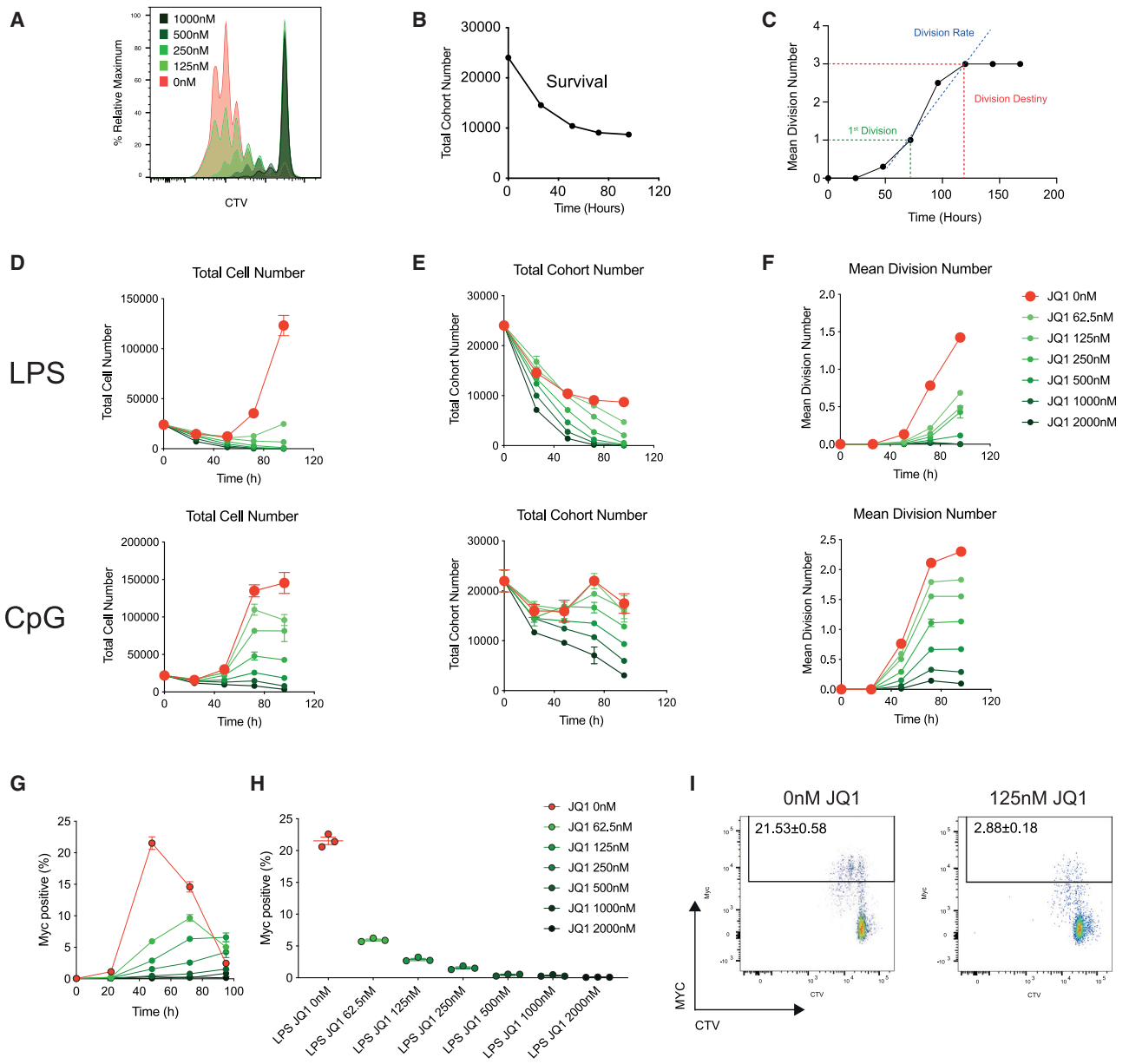

Figure 3. JQ1 Causes a Reduction in Proliferation and Survival of B Cells *In Vitro*

(A) Proliferation profiles of LPS-stimulated CTV-labeled B cells 4 days post-activation, with indicated concentrations of JQ1.

(B) Total cell numbers per division for data in (A) were determined by quantification to a known number of added beads and then corrected to reduce the effect of expansion, giving the total cohort number.

(C) Cohort analysis plot of mean division number (MDN) reveals division rate, time to first division, and division destiny.

(D–F) Total cell number (D), (E) total cohort number, and (F) MDN of B cells stimulated with LPS and CpG in thepresence of indicated concentrations of JQ1.

(G–I) Percentage of Myc expressing LPS-activated B cells over time (G) and (H) percentage of Myc^{+} cells at peak of expression (48hr). Representative plots of Myc-staining are shown in (I).

The data in (A)–(C) and (I) are representative plots from triplicate samples. The data in (D)–(I) are means ± SEMs of triplicate samples. All of the data are representative from 3 independent experiments.

transcription. To investigate whether the phenotypic effects of JQ1 are caused by global, preferential, or selective Brd4 displacement, we profiled genome-wide Brd4 occupancy via chromatin immunoprecipitation sequencing (ChIP-seq) over time in stimulated B cells. B cells were stimulated with LPS and treated with or without JQ1 for either 2 or 8 h, after which ChIP-seq was performed. The next-generation sequencing datasets were subsequently analyzed to identify Brd4 peaks

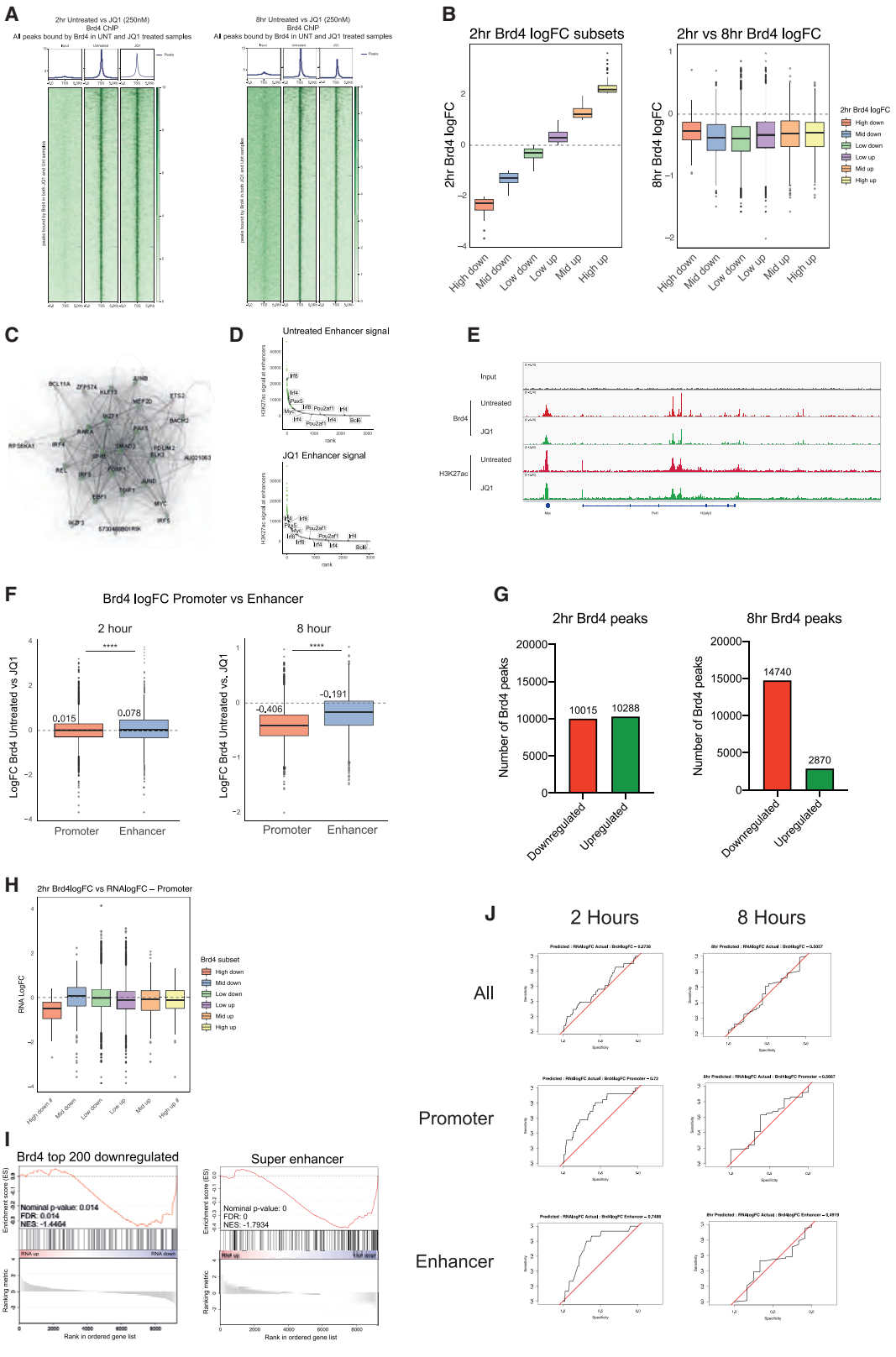

(legend on next page)

significantly enriched over background (input control), after which the Brd4 occupancy was quantified in these regions in a genome-wide manner (Figures 4A, S3A, and S3B). Visualization of Brd4 occupancy around Brd4 peak summits or transcriptional start site (TSS) proximal transcriptional units revealed minimal global displacement of Brd4 at 2 h, which increases significantly over time, resulting in the global loss of Brd4 occupancy in JQ1-treated conditions across all Brd4 peaks at TSS regions (Figure 4A). Specific genomic loci occupied by Brd4 are exquisitely sensitive to JQ1, although prolonged exposure results in the global loss of Brd4 binding (Figure 4B). To investigate the genomic context of Brd4-occupied sites, we performed ChIP-seq for histone 3 lysine 27 acetylation (H3K27ac), an epigenetic mark associated with active promoters and enhancers. This revealed a strong correlation between H3K27 acetylation levels and Brd4 occupancy (Figure S3C), with high levels of Brd4 and H3K27ac occurring at super-enhancer regions that drive the expression of key B cell genes such as Pax5 and Irf8. Integrated core transcriptional network analysis revealed that these enhancer networks impinge on a limited set of B cell transcription factors, which included *SpiB*, *Pax5*, *Ebf1*, *Bach2*, *Irf4*, and *Myc*. Using H3K27ac marks, we performed a network analysis to determine whether JQ1 preferentially targeted gene promoters or super-enhancers in JQ1-treated B cells at 2 h (Figure 4C). We observed no change in the enhancer signal at key genes associated with B cell function (Figure 4D) or the H3K27ac signal at the top 200 enhancers upon the addition of JQ1 (Figures S3D and S3E). Our analysis included genes previously implicated in Brd4 pathway interactions, perhaps best illustrated by the reduction in binding to *Myc* (Figure 4E). Analysis of Brd4 displacement across all H3K27ac-occupied sites revealed that displacement was selective 2 h post-JQ1 exposure, with both increased and decreased Brd4 occupancy (Figures 4F, 4G, and S3F). In contrast, within 8 h, Brd4 displacement was global, with a significant reduction in Brd4 occupancy across most loci, which was particularly prominent at promoter regions (Figures 4F, 4G, and S3F). To gain further mechanistic insight into the temporal relationship between Brd4 displacement and the transcriptional response to JQ1 we performed 3′ RNA sequencing (RNA-seq) at matching time points. Integration of the transcriptional and genomic data by the stratification of genes according to Brd4 displacement revealed a significant correlation between promoter-bound Brd4 displacement and the loss of transcription of the corresponding gene 2 h post-JQ1 treatment. This implies that the promoter displacement of Brd4 is the likely driver of acute JQ1 responses on the transcriptional level (Figure 4H). Gene set enrichment analysis (GSEA) demonstrated that the top 200 genes with Brd4 displacement correlated with the reduction in expression (Figure 4I). Accordingly, receiver-operating characteristic (ROC) analysis of the binarized JQ1 response and Brd4 displacement revealed that the loss of Brd4 binding at promoters and enhancers was predictive for subsequent transcriptional changes at 2 h post-JQ1 exposure (Figure 4J). In contrast, any correlation between transcriptional changes and Brd4 displacement was lost at 8 h of JQ1 exposure, when the displacement of Brd4 is global (Figures 4H and 4I).

An alternative explanation for the multi-parameter effect of JQ1 on B cell responses is that the observed levels of Brd4 displacement are sufficient to downregulate transcription at a global level, either directly or indirectly via the downregulation of Myc, which mediates global transcriptional amplification in B cells, resulting in increased RNA content per cell upon activation (Kieffer-Kwon et al., 2017). Therefore, we used Myc levels as a surrogate marker of the effect of JQ1 in B cell cultures. We addressed this hypothesis by measuring the effect of JQ1 on transcription rates (via incorporation of 5-ethynyl uridine [EU]) in relation to Myc expression at both the population level and relative to cell division (Figure S4). We observed a global increase in EU incorporation as B cells enter division, which fits with the notion that upon activation, there is an increase in cellular RNA content (Figure S4A). Consistent with our previous results, treatment with JQ1 in EU-pulsed cultures reduced the expression of Myc (Figure S4B) and delayed cell division (Figure S4C). However, JQ1 treatment did not lead to a reduction in the proportion of RNA-producing cells or RNA production (Figures S4D and S4E), until B cells reached their division destiny and were stalled in proliferation, as represented by the loss of Myc (Figures S4F and S4G). This effect of Myc loss and division destiny was also correlated with reduced transcription in cells

Figure 4. JQ1 Treatment Results in a Global Reduction in Brd4 Occupancy

ChIP-sequencing was performed to examine the Brd4 occupancy upon JQ1 treatment (250 nM).

(A) BRD4 occupancy across all BRD4 peaks between untreated and JQ1-treated samples at 2 and 8 h post-activation.

(B) Brd4 peaks were separated into clusters based on log fold change (logFC) upon JQ1 treatment at 2 h. High down (Brd4logFC < −2; 49 peaks), mid-down (Brd4logFC −2 to −1; 613 peaks), low down (Brd4logFC −1 to 0; 9,353 peaks), low up (Brd4logFC 0–1; 9,164 peaks), mid-up (Brd4logFC 1–2; 979 peaks), and high up (Brd4logFC > 2; 145 peaks). Brd4 logFCs at 8 h for each cluster were plotted.

(C) Transcription factor network of untreated samples.

(D) Super-enhancer signals for untreated and JQ1-treated samples highlighting transcription factors associated with Brd4 binding and B cells. Super-enhancers are highlighted in green.

(E) Brd4 and H3K27ac peak summits at *Myc* promoter and enhancer regions for untreated (red) and JQ1 (green) treated samples.

(F) FC of Brd4 occupancy between untreated and JQ1-treated samples (2 and 8 h post-treatment) at promoter and enhancer. Promoter region defined as <10,000 bp within TSS region and enhancer region defined by >10,000 bp from TSS region.

(G) Downregulated and upregulated Brd4 peaks in response to JQ1 treatment at 2 and 8 h.

(H) RNA logFC at 2 h for clusters in (B).

(I) GSEA analysis for top 200 downregulated Brd4 genes and super-enhancer genes in relation to RNAlogFC in response to JQ1 at 2 h.

(J) Receiver-operating characteristic (ROC) analysis of the downregulation of RNA and Brd4 displacement for all regions, promoter regions, and enhancer regions at 2 and 8 h.

Significance differences were determined using the Wilcoxon signed-rank test. ****$p \leq 0.0001$.

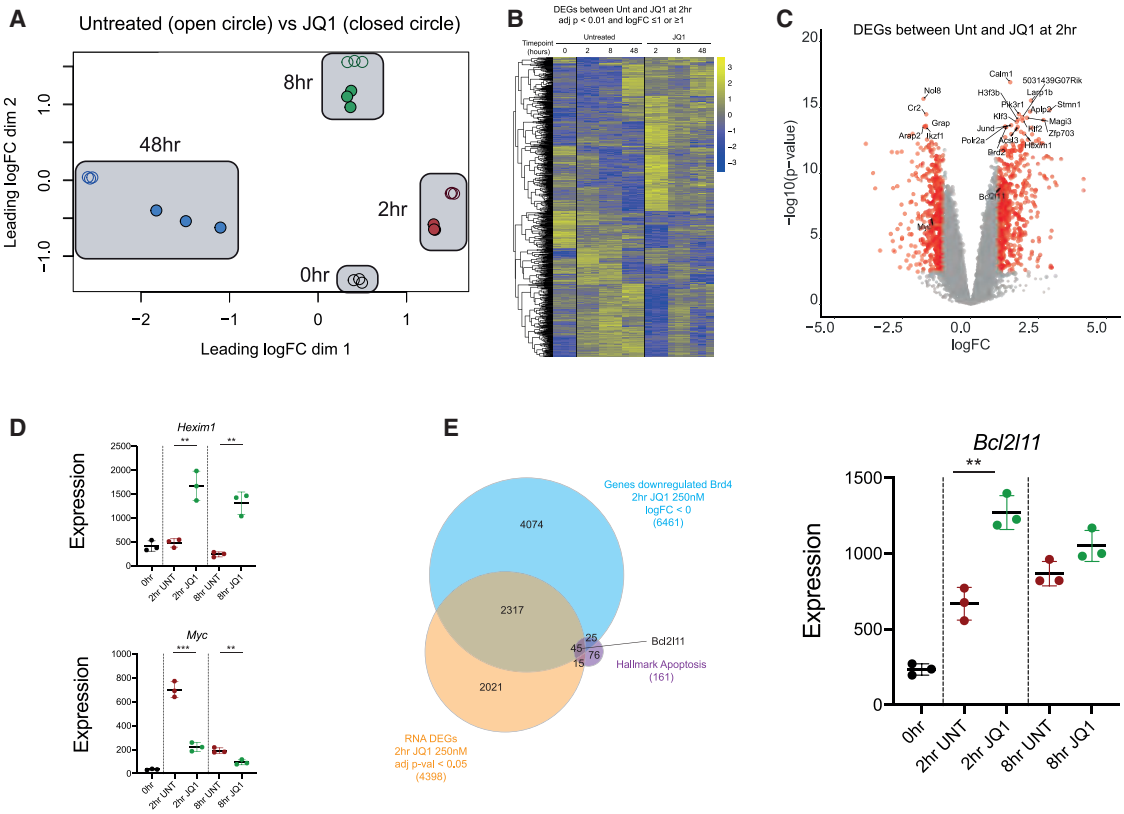

Figure 5. JQ1 Treatment Induces Genome-wide Changes in Gene Transcription

3′ RNA-seq analysis was performed on LPS-stimulated B cells with and without JQ1 (250 nM).

(A) Multidimensional scaling (MDS) plot for LPS-stimulated B cells with or without JQ1 treatment at 0, 2, 8, and 48 h.

(B) Gene expression heatmap of DEGs between untreated and JQ1-treated samples at 2 h (cutoff values logFC ≥ 1 or logFC ≤ 1 and adjusted p ≤ 0.01) for 0, 2, 8, and 48 h.

(C) Volcano plot for DEGs regulated by JQ1 in LPS-stimulated cells 2 h post-activation with cutoff values logFC ≥ 1 or logFC ≤ 1 and p value ≤ 0.05.

(D) Expression of *Hexim1* and *Myc* for untreated and JQ1-treated samples at 0, 2, and 8 h.

(E) Venn diagram showing DEGs regulated by JQ1, genes of differentially regulated Brd4 peaks by JQ1 treatment and HALLMARK_APOPTOSIS genes (Broad Institute MSigDB: M5902). Expression of *Bcl2l11* for untreated and JQ1-treated samples at 0, 2, and 8 h.

The data in (D) and (E) are means ± SEMs of triplicate samples. Significance differences were determined using unpaired Student's t test. **p ≤ 0.01 and ***p ≤ 0.001.

with Myc downregulation (Figure S4H). These results provide strong evidence that Brd4 displacement is promiscuous in the context of JQ1.

Treatment with JQ1 Induces Cell-Cycle and Cell Death Gene Expression Signatures

To identify gene-specific effects in response to JQ1, we performed a gene-level analysis of the 3′ RNA-seq datasets. We performed triplicate time course experiments analyzing gene expression at 2, 8, and 48 h post-stimulation with LPS stimulation (Figure 5) in the presence or absence of JQ1. Previous studies have shown that B cells undergo rapid transcriptional changes and chromatin remodeling post-activation, and these changes are almost completely imprinted from 24 h post-activation (Bouillet et al., 1999). Thus, we chose the early time points (2 and 8 h) and the late time point (48 h) to examine the direct effects of JQ1 on early and late changes in gene expression, respectively. As expected, JQ1 induced widespread changes in gene expression by 48 h. These changes in gene expression clustered in relation to time post-activation (Figure 5A), consistent with the LPS-induced transcriptional response. In addition, distinct subgroups clustered within each time point according to treatment with JQ1 (Figures 5A–5C: 1,071 differentially expressed genes [DEGs]). Importantly, DEG analysis of these datasets consistently detected changes in the gene expression of JQ1 targets such as *Hexim1* and *Myc* (Figure 5D).

We reasoned that a detailed analysis of DEGs from 2 h could identify mechanistic details about the response of activated B cells that were direct targets of JQ1 (namely, apoptosis and cell-cycle arrest). Gene Ontology analysis of DEGs revealed expected changes consistent with the findings presented in Figures 2, 3, and S5A, including lymphocyte homeostasis, regulation of cell-cycle arrest, and B cell activation, among others. This is further reflected by the positive enrichment of apoptosis and cell-cycle checkpoint genes via GSEA (Figures S5B and S5C). Surprisingly, despite the reduced antibody levels, we

measured no significant enrichment of antibody-secreting genes (Figure S5B). This supports our conclusion that the loss of antibody production in the context of JQ1 treatment is a combined result of altered B cell survival and proliferation, rather than direct targeting of transcriptional pathways related to plasma cell differentiation. To isolate candidate genes responsible for the pro-apoptotic effect of JQ1 on B cells (Figures 2 and 3), we cross-referenced DEG from our datasets with Gene Ontology associated with cell death, using the database HALLMARK_APOPTOSIS (161 genes). In addition, we compared this dataset with genes with differential Brd4 occupancy in response to 2 h of JQ1 treatment, as shown in Figure 4. Of particular interest, when we segregated shared genes between these lists, we identified 45 genes that overlapped between these criteria (Figure 5F). At 2 h, the predominant outcome we observed in overlapping datasets with DEGs was a significant increase in gene expression (Figures S5D and S5E). The curated gene list included the pro-apoptotic family member *Bcl2l11* (Bim, Figure 5F), which has been shown to play a crucial role in lymphocyte survival (Xu et al., 2016). This finding was of particular interest as JQ1 has been reported to upregulate Bim expression and induce apoptosis in non-activated B cell subsets such as pro-B cells, pre-B cells, and resting follicular B cells (Harris et al., 1988). Furthermore, similar findings have been observed in malignant B cells such as the Eμ-Myc mouse model of Burkitt lymphoma, in which the overexpression of Myc is driven and maintained by the IgH promoter (Lim et al., 2014). Thus, the constitutive expression of Myc allows this variable to be removed. Consistent with our analysis, the treatment of Eμ-Myc B cells *in vitro* with JQ1 leads to the differential expression of Bim (Figure S5F), as well as the displacement of Brd4 at both *Bim* and *Hexim1*, with a concomitant increase in gene transcription, as demonstrated by the increased binding of RNA Pol II (Figure S5G). Thus, our data provide strong evidence that JQ1-mediated changes in Bim are conserved between B cell subtypes. Data from both normal and transformed B cells suggest that *Bcl2l11* transcripts are induced or stabilized despite global Brd4 displacement. However, the contribution of JQ1-targeted pathways in the context of B cell activation and antibody production remains unexplored. In addition, we noted no significant trends in the expression of nuclear factor κB (NF-κB) subunits or binding of Brd4 to key B cell transcription factors directly driven by the effects of JQ1 on purified B cell cultures (Figures S5H and S5I). Therefore, we hypothesized that while JQ1 induced a number of changes in gene expression that contributed to the proliferation and differentiation compartments (which manifest as downstream changes in Myc levels as observed above), reduced cell survival could be attributed to the upregulation of the pro-apoptotic gene *Bcl2l11*.

JQ1 Treatment Induces Death in B Cells through the Upregulation of Bcl2l11 via a Compartment-Specific Effect

To establish whether the effects of JQ1 on cell death during antibody responses *in vitro* (Figures 2 and 3) could be attributed solely to the upregulation of the pro-apoptotic gene *Bcl2l11*, we performed a quantitative cohort analysis of JQ1-treated B cell cultures using B cells deficient for pro-apoptotic BH3-only protein family members. We investigated the response of Bim-deficient B cells (differentially expressed in response to JQ1 treatment) as well as Noxa- and Puma-deficient B cells (unaffected by JQ1 treatment) to LPS stimulation as performed previously (Figure 6; Table S3). JQ1-induced cell death was absent in $Bim^{-/-}$ B cell cultures (Figure 6B). This finding is illustrated in "total cohort plots" tracking founder cells over the 4-day culture period (Figure 6B versus Figure 6F). In the absence of Bim, JQ1-induced cell death was ablated and all founder cells remained traceable (Figure 6F), regardless of the JQ1 concentration used (Figures 6A and 6B versus Figures 6E and 6F). Despite the abrogation of cell death, JQ1 treatment still had a significant effect on cell division (measured by mean division number over time) and differentiation in $Bim^{-/-}$ (Figures 6C, 6D, and 6Q versus Figures 6G and 6H). In contrast, quantitative functional assays of B cells deficient for Noxa and Puma (unaffected by JQ1) were identical to wild-type B cells (Figures 6I–6P). These findings were consistent with the quantitative analysis of CpG-stimulated B cell cultures (Figure S6). Thus, the molecular mechanism of JQ1-mediated cell death during B cell activation and *in vitro* antibody production could be attributed solely to the gene *Bcl2l11* (Bim). In contrast, the effects of JQ1 on B activation and proliferation were independent of Bim. These findings suggest that distinct and independently regulated gene networks control these processes.

As our results suggested that non-selective downregulation of Myc was associated with reduced B cell proliferation and activation, we attempted to validate our finding that Myc controlled B cell activation and proliferation could be targeted independently of cell survival. We performed a quantitative analysis of B cells in response to treatment with CTX-0391034, which inhibits Myc expression via protein arginine methyltransferase 5 (PRMT5) due to the multifactorial role of PRMT5, including maintenance of Myc stability, recruitment of Myc to chromatin, and promotion of Myc translation (Mongiardi et al., 2015; Park et al., 2015; Chan-Penebre et al., 2015). CTX-0391034 is a potent and highly selective inhibitor of PRMT5 (Figures S7A and S7B) that has structural similarity to that previously reported by Chan-Penebre et al. (Wei et al., 2015). Interestingly, treatment with CTX-0391034 had no effect on cell survival, as represented by total cell numbers over the first 48 h in culture (Figures S7C and S7H) and tracking founder cells in cohort plots (Figures S7D and S7H). Instead, increasing concentrations of CTX-0391034 led to a significant reduction in progression through cell division (Figures S7E and S7H) and subsequent reduction in mean division number (Figure S7F) that occurred concomitantly with the decreased expression of Myc protein (Figures S7G and S7H). These results are consistent with the independent regulation of proliferation and survival compartments and support the conclusion that the effect of JQ1 on cell survival is mediated solely through Bim, while non-selective JQ1-mediated downregulation of Myc is associated with reduced B cell proliferation and cell division.

DISCUSSION

Therapeutic strategies targeting BET-bromodomains are emerging as potential new avenues for treating cancers and

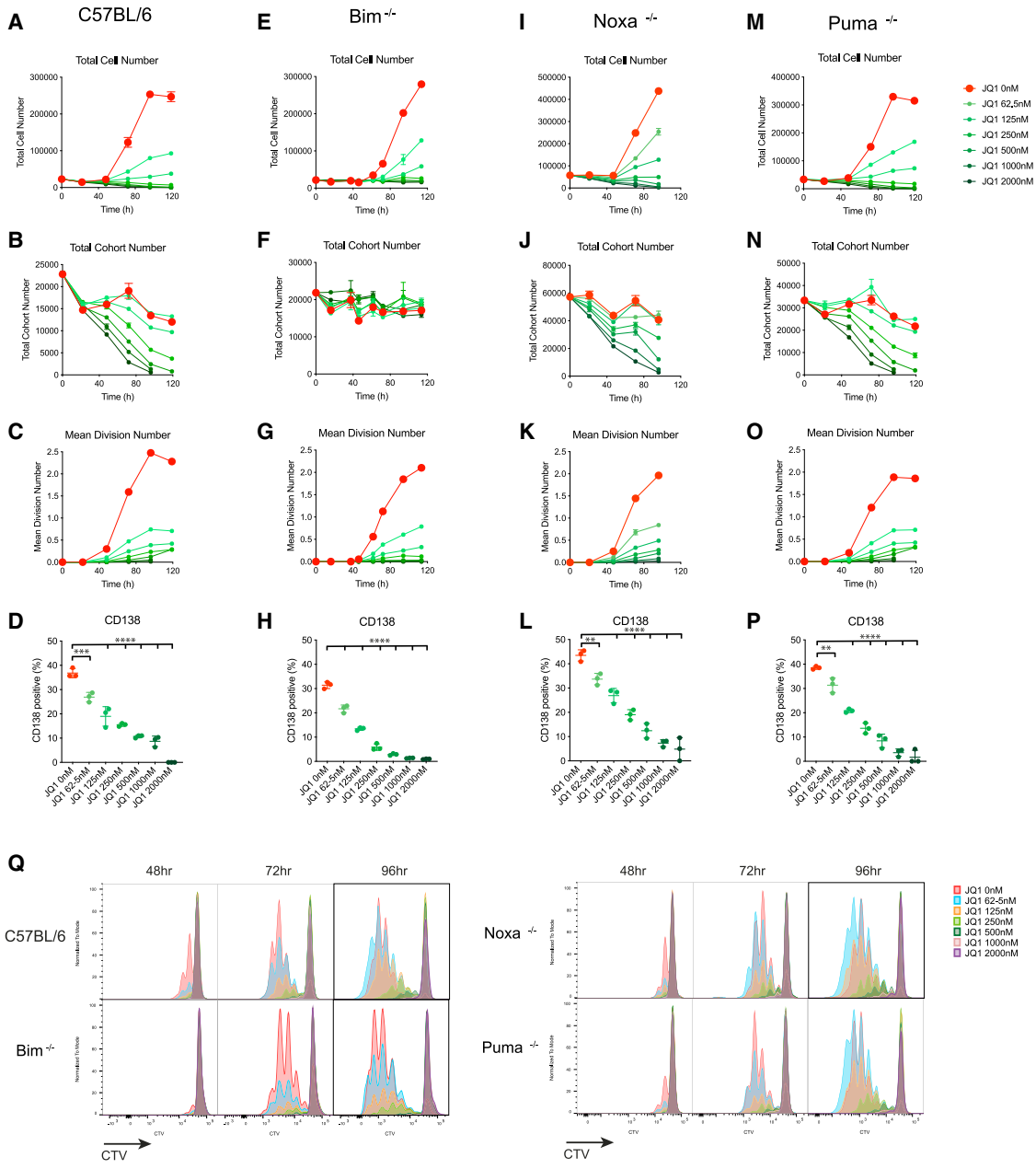

Figure 6. Deletion of *Bcl2l11* Rescues Cell Death as a Result of JQ1 Treatment

(A–P) Cohort analysis was performed on purified B cells stimulated with LPS. Total cell number, total cohort number, mean division number, and proportion of CD138^{+} cells were quantified for (A–D) C57BL/6, (E–H) Bim knockout (KO), (I–L) Noxa KO, and (M–P) Puma KO, respectively.

(Q) Representative CTV plots for all genotypes at 48, 72, and 96 h with indicated concentrations of JQ1.

All data are means ± SEMs of triplicate samples and are representative from 3 independent experiments. The data in (Q) are representative of triplicate samples. All of the statistical tests were performed in comparison to untreated control. Significance differences were determined using ANOVA Bonferroni corrections. **p ≤ 0.01, ***p ≤ 0.001, and ****p ≤ 0.0001.

immune disorders. However, the effect of many BET inhibitors such as JQ1 on the protective immune system is not well understood. Similarly, the precise molecular mechanism that drives changes in cell fate in the context of epigenetic modifiers is unclear. Here, we applied a system-wide compartmentalized approach to study how JQ1 can affect protective antibody responses. We paired quantitative functional measurements with genome-wide molecular analysis to identify JQ1-mediated changes in gene expression and assigned them to the underlying protective function of B cells (summarized in Figure 7). Our data illustrate that JQ1 has a significant effect on humoral immune responses through targeting B cells directly. The overall antibody

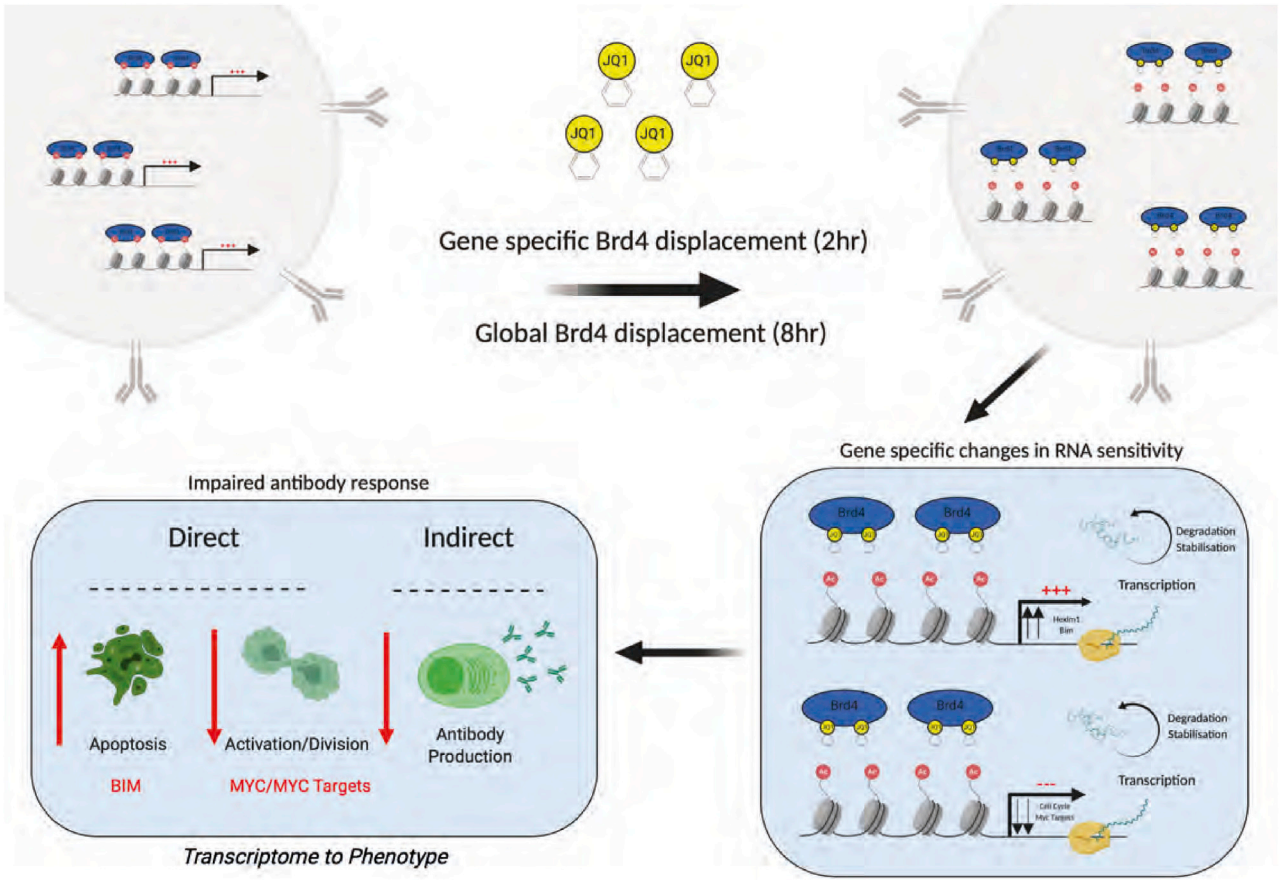

Figure 7. JQ1-Mediated Changes in B Cell Function

JQ1 affects multiple parameters of B cell function via the global displacement of Brd4. This results in subsequent changes in gene transcription irrespective of Brd4 displacement. Our results suggest that gene selectivity occurs at the post-transcriptional level (e.g., RNA degradation). By combining quantitative analysis with genomic studies, we have shown that the regulation of apoptosis by JQ1 is mediated solely through the pro-apoptotic protein Bim. Conversely, the regulation of the cell cycle by JQ1 is linked to the downregulation of Myc-associated genes. This combined effect in the context of B cells leads to a JQ1-mediated downregulation of antibody production.

response was significantly inhibited by JQ1 treatment as a result of the combined reduction of cell survival, initial activation, cell division, and isotype switching. As B cell differentiation is division linked, the impact of JQ1 on antibody production could be attributed directly to the changes described above as opposed to the B cell ASC differentiation compartments that were not affected.

Consistent with these effects, there is emerging evidence that JQ1 can modify the immune responses and diseases of the immune system, including autoimmune diseases. JQ1 has been shown to reduce cytokine and anti-double-stranded DNA (dsDNA) antibody levels in the MRL/*lpr* model of lupus (Wei et al., 2015) (similar to models we have used here). The therapeutic effects in this context have largely been attributed to modifying the inflammatory landscape by enhancing the production of suppressive cytokines such as IL-10 and IL-17 (Lee et al., 2017). This is somewhat at odds with reports that in regulatory B cells, JQ1 treatment leads to reduced IL-10 production by disrupting the interactions of Brd4 directly at its promoter site (Lee et al., 2017). Furthermore, it has been reported that in response to LPS, JQ1 mediates its effects through the specific targeting of NF-κB subunits (discussed below) (Tyler et al., 2017). Our results question these interpretations. We show that JQ1 induces the rapid cell death of B cells, stalls their proliferation, and alters isotype switching *in vitro*. This is consistent with the direct effects of JQ1 on the B cell lineage in contrast to the proposed indirect mechanisms discussed above. In line with these results, in B6.MRL/*lpr* mice, we demonstrate a significant loss of B cells and plasma cell subsets in blood and peripheral lymphoid organs. However, myeloid cells and both CD4 and CD8 T cell populations were also significantly reduced, with little preference for activated or naive lineages. Given the role of these immune cells supporting survival and expansion of B cell populations in both protective (immunization) and pathogenic (autoimmune) settings, it is likely that the *in vivo* effects of JQ1 are a result of the synergistic effects on interacting immune cell subsets. An exception to the efficacy of JQ1 *in vivo* was in the bone marrow, where little effect on the B cell lineage was measured. This result is consistent with studies in hematopoietic lineage cancers that demonstrate using a chemically modified version that JQ1 is

readily detectable in cancer cells circulating in blood, spleen, and lymph nodes, but uptake in tumor cells located in the bone marrow is reduced significantly (Kieffer-Kwon et al., 2017). We also demonstrate that although acute responses (within 2 h) are selective, Brd4 is displaced in a global manner within 8 h in B cells that is thereafter maintained long term. This is consistent with supporting evidence that epigenetic programming (largely dependent on Myc-induced changes) of primary B cells is dynamic and programmed long term within the first 24 h following stimulation (Gao et al., 2015). Therefore, mechanisms regarding specific targeting of NF-κb subunits or specific cytokines are inconsistent with the conditions tested here. The effect of Brd4 displacement on NF-κb subunits in the context of immunization in which antibody responses are impaired (Chapuy et al., 2013) or targeting of GC-associated transcription factors in B cell malignancies has previously been reported (Delmore et al., 2011). Our temporal analysis of key B cell GC transcription factors (Irf8, Pax5, Pou2af1, Irf4, and Bcl6) demonstrated no preferential changes after treatment with JQ1, in contrast to studies with diffuse large B cell lymphoma, although subtle fluctuations with no discernable trend were noted in NF-κb subunits over time (Figures S5G and S5H). Thus, our results suggest that changes in proliferation induced by JQ1 lead to significant changes in B cell differentiation, most likely due to the division-linked nature of this process.

JQ1 has been proposed to exert its biological effects by displacing Brd4 in a gene-specific manner, thereby resulting in targeted outcomes such as reduced proliferation or induction of cell death (Muhar et al., 2018). Our results demonstrate an initial dependency on gene selectivity. We find that over a 4-day quantitative assay measuring the antibody response, Brd4 displacement occurs in a gene-specific manner within 2 h of stimulation and JQ1 treatment. However, this specificity is lost within 8 h when Brd4 is globally displaced (Figure 4). In addition, we did not observe a significant downregulation of gene expression at the population level, driven by Brd4 displacement or downregulation of Myc at the protein level. Thus, an alternative hypothesis to reconcile our findings with previous studies is that gene selectivity occurs at the post-transcriptional level or is determined by gene-intrinsic factors affecting Pol II-pausing ratios and RNA production rates. This is in agreement with recent findings by Zuber and colleagues that demonstrate that low-dose JQ1 results in gene-selective effects despite the global displacement of BRD4, which was observed to be associated with multiple gene-specific parameters such as SUPT5H occupancy at the promoter and H3K27ac levels (Sabò et al., 2014). Interestingly, despite the downregulation of Myc expression, JQ1 treatment had little effect on the global RNA output of the cell at the population level as measured by EU incorporation. These results suggest that the effect of JQ1 on B cell responses is not mediated by a global Brd4 displacement and overall downregulation of transcription. This supports the idea that gene-intrinsic properties result in an apparent selective response at the transcriptional level in spite of global Brd4 displacement. Interestingly, our data also demonstrate that global RNA production is unaffected by the acute downregulation of Myc. This is in line with recent studies demonstrating that the transcriptional increase driven by Myc results from changes in a limited number of genes (~750) rather than promiscuous global transcriptional amplification across all genes (Heinzel et al., 2017). The only exception we found was a reduction in transcription rates in B cells with division progression stalled by JQ1. In this scenario, EU incorporation occurred concomitantly with the downregulation of Myc as B cells reached division destiny, a previously described autonomous response that regulates long-term B cell expansion and identified earlier as an effect targeted by JQ1 (Bissonnette et al., 1992). In many systems, Myc has been implicated to influence cell death (Shi et al., 1992; Waibel et al., 2018). However, in this context, we demonstrate that changes in Myc levels are not associated with cell death. This is perhaps most striking in $Bim^{-/-}$ B cells treated with JQ1 that are completely protected from cell death. Using a PRMT5 inhibitor, we show that Myc is most likely a downstream amplifier of the response to JQ1 with regard to proliferation, as levels of Brd4 displacement at Myc and transcript levels are not specifically targeted by JQ1. These results are consistent with recent studies using HDACi. Here, panobinostat was shown to reduce the proliferation of T cell acute lymphoblastic leukemia cells as a result of the indirect downregulation of Myc induced by targeting drivers of the oncogenic signature rather than Myc itself (Hogg et al., 2017). Similarly, in the transgenic Eμ-Myc B cell lymphoma model, *Myc* transcript levels are unaffected by JQ1 treatment and global Brd4 displacement, but nonetheless a Myc signature and significant transcriptional response can still be observed, providing further evidence that Myc transcriptional networks can be disrupted in the absence of Myc downregulation (Hawkins et al., 2013b).

The complete segregation of the effects of JQ1 on cell survival from the effects on proliferation and differentiation were striking and highlight a number of points. It is a strong example that these contrasting processes can be compartmentalized for analysis at both the functional and mechanistic levels. Although they are often discussed as interleaved, there is accumulating evidence that individual compartments embodied by the Cyton model are independently regulated, whether in response to levels/types of stimulation (Waibel et al., 2015), drug treatments (Waibel et al., 2015), or in gene-deficient models (as shown here). Therefore, there is a pressing need to identify therapeutics that can enhance or inhibit a single compartment (proliferation/survival/differentiation), as we have previously identified (Hawkins et al., 2007a). For example, identifying a compound that is capable of enhancing or reducing antibody production alone would be applicable to most immunodeficiencies or B cell-mediated autoimmune conditions, respectively. Similarly, we believe that this provides a powerful approach to identifying more effective synergistic therapeutic strategies. Using compounds that have been quantified and shown to enhance (or inhibit) separate Cyton compartments of target cells offers the ability to design therapeutics approaches with genuine synergy.

In summary, this study illustrates the compartmentalized molecular regulation of fundamental components of immune cell biology and how quantitative techniques combining cell biology with transcriptomics are a powerful approach that allow these effects to be dissected. The next step is identifying combination therapies that address distinct pathways or epigenetic machinery, thus providing a powerful quantitative platform to predict

enhanced or decreased immunity. This could take the reverse approach we have applied to study mechanisms of epigenetic modifying compounds. For example, by screening mutations in epigenetic machinery in patients with immune disorders, similar quantitative assays could be applied to assign specific mechanisms to modified lymphocyte function. Our results illustrate the strength of *in vitro* reductionist systems that combine functional analysis of cell biology with genomics to isolate molecular mechanisms that regulate immunity.

STAR★METHODS

Detailed methods are provided in the online version of this paper and include the following:

- KEY RESOURCES TABLE
- RESOURCE AVAILABILITY
  - Lead Contact
  - Materials Availability
  - Data and Code Availability
- EXPERIMENTAL MODEL AND SUBJECT DETAILS
- METHOD DETAILS
  - Cell culture
  - Quantitative analysis
  - *In vitro* drug preparation
  - Intracellular staining of Myc
  - Intracellular staining of nascent RNA
  - ELISA assays
  - RNA sequencing and analysis
  - ChIP-Sequencing and analysis
  - Super enhancer analysis
  - *In vivo* JQ1 therapy
  - Synthesis of CTX-0391034
- QUANTIFICATION AND STATISTICAL ANALYSIS

SUPPLEMENTAL INFORMATION

Supplemental Information can be found online at https://doi.org/10.1016/j.celrep.2020.108290.

ACKNOWLEDGMENTS

We thank Professor Steve Nutt, A/Prof. Marnie Blewitt, and A/Prof. Anne Voss for constructive criticism on the manuscript. We would like to thank Lisa Reid, Rhiannan Crawley, and Rebekah Meeny for animal husbandry. J.S.R. was supported by an Australia Postgraduate Award. E.D.H. was supported by a R.D. Wright career development fellowship (1159488) from the National Health and Medical Research Council of Australia (NHMRC) and grants from The Leukemia & Lymphoma Society (6552-18) and NHMRC (1140187 and 1165591). This work was made possible through Victorian State Government Operational Infrastructure Support and Australian Government NHMRC Independent Research Institutes Infrastructure Support Scheme Grant 361646. Work from the Johnstone lab (R.W.J.) was supported by the Cancer Council Victoria, the NHMRC, and The Kids' Cancer Project. The Peter MacCallum Foundation and the Australian Cancer Research Foundation provided generous support for equipment and core facilities.

AUTHOR CONTRIBUTIONS

S.J.V. and E.D.H. conceived the project. I.Y.K., J.S.R., A.L., S.J., and D.A.K. performed the experiments. J.S.R. and I.Y.K. performed the *in vitro* quantitative analysis. S.J. and E.M. performed the ANA analysis. B.J.M., S.H., and P.B. provided the reagents and intellectual input on the experimental design. I.Y.K. and S.J.V. performed the genomic analysis. I.T. performed the super-enhancer analysis. S.J.H. performed the analysis on the Eμ-Myc cells. I.Y.K. and A.L. maintained all of the animal lines. I.Y.K., J.S.R., S.J.V. and E.D.H. analyzed the data and wrote the manuscript. Every author contributed revisions to the manuscript. The study was overseen and expert input was provided by R.W.J. and P.D.H.

DECLARATION OF INTERESTS

The laboratory of R.W.J. receives research support from F. Hoffmann-La Roche, Bristol-Myers Squibb, and MecRx. R.W.J. is a scientific consultant and shareholder in MecRx.

Received: October 18, 2019
Revised: May 24, 2020
Accepted: September 29, 2020
Published: October 20, 2020

REFERENCES

Adams, J.M., Harris, A.W., Pinkert, C.A., Corcoran, L.M., Alexander, W.S., Cory, S., Palmiter, R.D., and Brinster, R.L. (1985). The c-myc oncogene driven by immunoglobulin enhancers induces lymphoid malignancy in transgenic mice. Nature *318*, 533–538.

Baell, J.B., Leaver, D.J., Hermans, S.J., Kelly, G.L., Brennan, M.S., Downer, N.L., Nguyen, N., Wichmann, J., McRae, H.M., Yang, Y., et al. (2018). Inhibitors of histone acetyltransferases KAT6A/B induce senescence and arrest tumour growth. Nature *560*, 253–257.

Bissonnette, R.P., Echeverri, F., Mahboubi, A., and Green, D.R. (1992). Apoptotic cell death induced by c-myc is inhibited by bcl-2. Nature *359*, 552–554.

Bouillet, P., Metcalf, D., Huang, D.C., Tarlinton, D.M., Kay, T.W., Köntgen, F., Adams, J.M., and Strasser, A. (1999). Proapoptotic Bcl-2 relative Bim required for certain apoptotic responses, leukocyte homeostasis, and to preclude autoimmunity. Science *286*, 1735–1738.

Burnet, F.M. (1976). A modification of Jerne's theory of antibody production using the concept of clonal selection. CA Cancer J. Clin. *26*, 119–121.

Chan-Penebre, E., Kuplast, K.G., Majer, C.R., Boriack-Sjodin, P.A., Wigle, T.J., Johnston, L.D., Rioux, N., Munchhof, M.J., Jin, L., Jacques, S.L., et al. (2015). A selective inhibitor of PRMT5 with in vivo and in vitro potency in MCL models. Nat. Chem. Biol. *11*, 432–437.

Chapuy, B., McKeown, M.R., Lin, C.Y., Monti, S., Roemer, M.G., Qi, J., Rahl, P.B., Sun, H.H., Yeda, K.T., Doench, J.G., et al. (2013). Discovery and characterization of super-enhancer-associated dependencies in diffuse large B cell lymphoma. Cancer Cell *24*, 777–790.

Deenick, E.K., Hasbold, J., and Hodgkin, P.D. (1999). Switching to IgG3, IgG2b, and IgA is division linked and independent, revealing a stochastic framework for describing differentiation. J. Immunol. *163*, 4707–4714.

Delmore, J.E., Issa, G.C., Lemieux, M.E., Rahl, P.B., Shi, J., Jacobs, H.M., Kastritis, E., Gilpatrick, T., Paranal, R.M., Qi, J., et al. (2011). BET bromodomain inhibition as a therapeutic strategy to target c-Myc. Cell *146*, 904–917.

Díaz, T., Rodríguez, V., Lozano, E., Mena, M.P., Calderón, M., Rosiñol, L., Martínez, A., Tovar, N., Pérez-Galán, P., Bladé, J., et al. (2017). The BET bromodomain inhibitor CPI203 improves lenalidomide and dexamethasone activity in *in vitro* and *in vivo* models of multiple myeloma by blockade of Ikaros and MYC signaling. Haematologica *102*, 1776–1784.

Dowling, M.R., Kan, A., Heinzel, S., Marchingo, J.M., Hodgkin, P.D., and Hawkins, E.D. (2018). Regulatory T Cells Suppress Effector T Cell Proliferation by Limiting Division Destiny. Front. Immunol. *9*, 2461.

Duffy, K.R., Wellard, C.J., Markham, J.F., Zhou, J.H., Holmberg, R., Hawkins, E.D., Hasbold, J., Dowling, M.R., and Hodgkin, P.D. (2012). Activation-induced

B cell fates are selected by intracellular stochastic competition. Science *335*, 338–341.

Filippakopoulos, P., Qi, J., Picaud, S., Shen, Y., Smith, W.B., Fedorov, O., Morse, E.M., Keates, T., Hickman, T.T., Felletar, I., et al. (2010). Selective inhibition of BET bromodomains. Nature *468*, 1067–1073.

Fong, C.Y., Gilan, O., Lam, E.Y., Rubin, A.F., Ftouni, S., Tyler, D., Stanley, K., Sinha, D., Yeh, P., Morison, J., et al. (2015). BET inhibitor resistance emerges from leukaemia stem cells. Nature *525*, 538–542.

Gao, F., Yang, Y., Wang, Z., Gao, X., and Zheng, B. (2015). BRAD4 plays a critical role in germinal center response by regulating Bcl-6 and NF-κB activation. Cell. Immunol. *294*, 1–8.

Gilan, O., Lam, E.Y., Becher, I., Lugo, D., Cannizzaro, E., Joberty, G., Ward, A., Wiese, M., Fong, C.Y., Ftouni, S., et al. (2016). Functional interdependence of BRD4 and DOT1L in MLL leukemia. Nat. Struct. Mol. Biol. *23*, 673–681.

Harris, A.W., Pinkert, C.A., Crawford, M., Langdon, W.Y., Brinster, R.L., and Adams, J.M. (1988). The E mu-myc transgenic mouse. A model for high-incidence spontaneous lymphoma and leukemia of early B cells. J. Exp. Med. *167*, 353–371.

Hasbold, J., Corcoran, L.M., Tarlinton, D.M., Tangye, S.G., and Hodgkin, P.D. (2004). Evidence from the generation of immunoglobulin G-secreting cells that stochastic mechanisms regulate lymphocyte differentiation. Nat. Immunol. *5*, 55–63.

Hawkins, E.D., Hommel, M., Turner, M.L., Battye, F.L., Markham, J.F., and Hodgkin, P.D. (2007a). Measuring lymphocyte proliferation, survival and differentiation using CFSE time-series data. Nat. Protoc. *2*, 2057–2067.

Hawkins, E.D., Turner, M.L., Dowling, M.R., van Gend, C., and Hodgkin, P.D. (2007b). A model of immune regulation as a consequence of randomized lymphocyte division and death times. Proc. Natl. Acad. Sci. USA *104*, 5032–5037.

Hawkins, E.D., Oliaro, J., Kallies, A., Belz, G.T., Filby, A., Hogan, T., Haynes, N., Ramsbottom, K.M., Van Ham, V., Kinwell, T., et al. (2013a). Regulation of asymmetric cell division and polarity by Scribble is not required for humoral immunity. Nat. Commun. *4*, 1801.

Hawkins, E.D., Turner, M.L., Wellard, C.J., Zhou, J.H., Dowling, M.R., and Hodgkin, P.D. (2013b). Quantal and graded stimulation of B lymphocytes as alternative strategies for regulating adaptive immune responses. Nat. Commun. *4*, 2406.

Heinz, S., Benner, C., Spann, N., Bertolino, E., et al. (2010). Simple Combinations of Lineage-Determining Transcription Factors Prime cis-Regulatory Elements Required for Macrophage and B Cell Identities. Mol Cell *38*, 576–589.

Heinzel, S., Binh Giang, T., Kan, A., Marchingo, J.M., Lye, B.K., Corcoran, L.M., and Hodgkin, P.D. (2017). A Myc-dependent division timer complements a cell-death timer to regulate T cell and B cell responses. Nat. Immunol. *18*, 96–103.

Hogg, S.J., Vervoort, S.J., Deswal, S., Ott, C.J., Li, J., Cluse, L.A., Beavis, P.A., Darcy, P.K., Martin, B.P., Spencer, A., et al. (2017). BET-Bromodomain Inhibitors Engage the Host Immune System and Regulate Expression of the Immune Checkpoint Ligand PD-L1. Cell Rep. *18*, 2162–2174.

Kagoya, Y., Nakatsugawa, M., Yamashita, Y., Ochi, T., Guo, T., Anczurowski, M., Saso, K., Butler, M.O., Arrowsmith, C.H., and Hirano, N. (2016). BET bromodomain inhibition enhances T cell persistence and function in adoptive immunotherapy models. J. Clin. Invest. *126*, 3479–3494.

Kieffer-Kwon, K.R., Nimura, K., Rao, S.S.P., Xu, J., Jung, S., Pekowska, A., Dose, M., Stevens, E., Mathe, E., Dong, P., et al. (2017). Myc Regulates Chromatin Decompaction and Nuclear Architecture during B Cell Activation. Mol. Cell *67*, 566–578.e10.

Kim, D., Paggi, J., Park, C., Bennett, C., and Salzberg, S. (2019). Graph-based genome alignment and genotyping with HISAT2 and HISAT-genotype. Nat biotechnol *37*, 907–915.

Langmead, B., and Salzberg, S. (2012). Fast gapped-read alignment with Bowtie 2. Nat Methods *9*, 357–359.

Law, C.W., Chen, Y., Shi, W., and Smyth, G.K. (2014). voom: precision weights unlock linear model analysis tools for RNA-seq read counts. Genome Biol. *15*, R29.

Lee, M.B., Lee, J.H., Hong, S.H., You, J.S., Nam, S.T., Kim, H.W., Park, Y.H., Lee, D., Min, K.Y., Park, Y.M., et al. (2017). JQ1, a BET inhibitor, controls TLR4-induced IL-10 production in regulatory B cells by BRD4-NF-κB axis. BMB Rep. *50*, 640–646.

Li, H., Handsaker, B., Wysoker, A., Fennell, T., Ruan, J., Homer, N., Marth, G., Abecasis, G., and Durbin, R.; 1000 Genome Project Data Processing Subgroup (2009). The Sequence Alignment/Map format and SAMtools. Bioinformatics *25*, 2078–2079.

Liao, Y., Smyth, G.K., and Shi, W. (2014). featureCounts: an efficient general purpose program for assigning sequence reads to genomic features. Bioinformatics *30*, 923–930.

Liberzon, A., Birger, C., Thorvaldsdóttir, H., Ghandi, M., Mesirov, J.P., and Tamayo, P. (2015). The Molecular Signatures Database (MSigDB) hallmark gene set collection. Cell Syst. *1*, 417–425.

Lim, J.H., Lee, Y.M., Lee, G., Choi, Y.J., Lim, B.O., Kim, Y.J., Choi, D.K., and Park, J.W. (2014). PRMT5 is essential for the eIF4E-mediated 5′-cap dependent translation. Biochem. Biophys. Res. Commun. *452*, 1016–1021.

Lun, A.T.L., and Smyth, G.K. (2016). csaw: a Bioconductor package for differential binding analysis of ChIP-seq data using sliding windows. Nucleic acids research. Nucleic acids research *44*. https://doi.org/10.1093/nar/gkv1191.

Markham, J.F., Wellard, C.J., Hawkins, E.D., Duffy, K.R., and Hodgkin, P.D. (2010). A minimum of two distinct heritable factors are required to explain correlation structures in proliferating lymphocytes. J. R. Soc. Interface *7*, 1049–1059.

Martin, M. (2011). Cutadapt removes adapter sequences from high-throughput sequencing reads. EMBnet.journal. https://doi.org/10.14806/ej.17.1.200.

Mertz, J.A., Conery, A.R., Bryant, B.M., Sandy, P., Balasubramanian, S., Mele, D.A., Bergeron, L., and Sims, R.J., 3rd. (2011). Targeting MYC dependence in cancer by inhibiting BET bromodomains. Proc. Natl. Acad. Sci. USA *108*, 16669–16674.

Mongiardi, M.P., Savino, M., Bartoli, L., Beji, S., Nanni, S., Scagnoli, F., Falchetti, M.L., Favia, A., Farsetti, A., Levi, A., et al. (2015). Myc and Omomyc functionally associate with the Protein Arginine Methyltransferase 5 (PRMT5) in glioblastoma cells. Sci. Rep. *5*, 15494.

Mootha, V.K., Lindgren, C.M., Eriksson, K.F., Subramanian, A., Sihag, S., Lehar, J., Puigserver, P., Carlsson, E., Ridderstrale, M., Laurila, E., et al. (2003). PGC-1alpha-responsive genes involved in oxidative phosphorylation are coordinately downregulated in human diabetes. Nat Genet *34*, 267–273.

Muhar, M., Ebert, A., Neumann, T., Umkehrer, C., Jude, J., Wieshofer, C., Rescheneder, P., Lipp, J.J., Herzog, V.A., Reichholf, B., et al. (2018). SLAM-seq defines direct gene-regulatory functions of the BRD4-MYC axis. Science *360*, 800–805.

Park, J.H., Szemes, M., Vieira, G.C., Melegh, Z., Malik, S., Heesom, K.J., Von Wallwitz-Freitas, L., Greenhough, A., Brown, K.W., Zheng, Y.G., et al. (2015). Protein arginine methyltransferase 5 is a key regulator of the MYCN oncoprotein in neuroblastoma cells. Mol. Oncol. *9*, 617–627.

Patel, M.C., Debrosse, M., Smith, M., Dey, A., Huynh, W., Sarai, N., Heightman, T.D., Tamura, T., and Ozato, K. (2013). BRD4 coordinates recruitment of pause release factor P-TEFb and the pausing complex NELF/DSIF to regulate transcription elongation of interferon-stimulated genes. Mol. Cell. Biol. *33*, 2497–2507.

Peeters, J.G., Vervoort, S.J., Mijnheer, G., de Roock, S., Vastert, S.J., Nieuwenhuis, E.E., van Wijk, F., Prakken, B.J., Mokry, M., and van Loosdregt, J. (2015). Autoimmune disease-associated gene expression is reduced by BET-inhibition. Genom. Data *7*, 14–17.

Rathert, P., Roth, M., Neumann, T., Muerdter, F., Roe, J.S., Muhar, M., Deswal, S., Cerny-Reiterer, S., Peter, B., Jude, J., et al. (2015). Transcriptional plasticity promotes primary and acquired resistance to BET inhibition. Nature *525*, 543–547.

Rizzitelli, A., Hawkins, E., Todd, H., Hodgkin, P.D., and Shortman, K. (2006). The proliferative response of CD4 T cells to steady-state CD8+ dendritic cells is restricted by post-activation death. Int. Immunol. *18*, 415–423.

Sabò, A., Kress, T.R., Pelizzola, M., de Pretis, S., Gorski, M.M., Tesi, A., Morelli, M.J., Bora, P., Doni, M., Verrecchia, A., et al. (2014). Selective transcriptional regulation by Myc in cellular growth control and lymphomagenesis. Nature *511*, 488–492.

Shi, Y., Glynn, J.M., Guilbert, L.J., Cotter, T.G., Bissonnette, R.P., and Green, D.R. (1992). Role for c-myc in activation-induced apoptotic cell death in T cell hybridomas. Science *257*, 212–214.

Stathis, A., and Bertoni, F. (2018). BET Proteins as Targets for Anticancer Treatment. Cancer Discov. *8*, 24–36.

Subramanian, A., Tamayo, P., Mootha, V.K., Mukherjee, S., Ebert, B.L., Gillette, M.A., Paulovich, A., Pomeroy, S.L., Golub, T.R., Lander, E.S., and Mesirov, J.P. (2005). Gene set enrichment analysis: a knowledge-based approach for interpreting genome-wide expression profiles. Proc. Natl. Acad. Sci. USA *102*, 15545–15550.

Turner, M.L., Hawkins, E.D., and Hodgkin, P.D. (2008). Quantitative regulation of B cell division destiny by signal strength. J. Immunol. *181*, 374–382.

Tyler, D.S., Vappiani, J., Cañeque, T., Lam, E.Y.N., Ward, A., Gilan, O., Chan, Y.C., Hienzsch, A., Rutkowska, A., Werner, T., et al. (2017). Click chemistry enables preclinical evaluation of targeted epigenetic therapies. Science *356*, 1397–1401.

Villunger, A., Michalak, E., Coultas, L., Mullauer, F., Bock, G., Ausserlechner, M., Adams, J.M., and Strasser, A. (2003). p53- and drug-induced apoptotic responses mediated by BH3-only proteins puma and noxa. Science *302*, 1036–1038.

Waibel, M., Christiansen, A.J., Hibbs, M.L., Shortt, J., Jones, S.A., Simpson, I., Light, A., O'Donnell, K., Morand, E.F., Tarlinton, D.M., et al. (2015). Manipulation of B-cell responses with histone deacetylase inhibitors. Nat. Commun. *6*, 6838.

Waibel, M., Vervoort, S.J., Kong, I.Y., Heinzel, S., Ramsbottom, K.M., Martin, B.P., Hawkins, E.D., and Johnstone, R.W. (2018). Epigenetic targeting of Notch1-driven transcription using the HDACi panobinostat is a potential therapy against T-cell acute lymphoblastic leukemia. Leukemia *32*, 237–241.

Watanabe-Fukunaga, R., Brannan, C.I., Copeland, N.G., Jenkins, N.A., and Nagata, S. (1992). Lymphoproliferation disorder in mice explained by defects in Fas antigen that mediates apoptosis. Nature *356*, 314–317.

Wei, S., Sun, Y., and Sha, H. (2015). Therapeutic targeting of BET protein BRD4 delays murine lupus. Int. Immunopharmacol. *29*, 314–319.

Xu, Z., Sharp, P.P., Yao, Y., Segal, D., Ang, C.H., Khaw, S.L., Aubrey, B.J., Gong, J., Kelly, G.L., Herold, M.J., et al. (2016). BET inhibition represses miR17-92 to drive BIM-initiated apoptosis of normal and transformed hematopoietic cells. Leukemia *30*, 1531–1541.

Zhang, Y., Liu, T., Meyer, C., et al. (2008). Model-based Analysis of ChIP-Seq (MACS). Genome Biol. https://doi.org/10.1186/gb-2008-9-9-r137.

Zuber, J., Shi, J., Wang, E., Rappaport, A.R., Herrmann, H., Sison, E.A., Magoon, D., Qi, J., Blatt, K., Wunderlich, M., et al. (2011). RNAi screen identifies Brd4 as a therapeutic target in acute myeloid leukaemia. Nature *478*, 524–528.

STAR★METHODS

KEY RESOURCES TABLE

REAGENT or RESOURCE	SOURCE	IDENTIFIER
Antibodies		
Rat anti-mouse CD45R/B220 (APC)	BD PharMingen	Cat# 553092; RRID:AB_398531
Rat Anti-mouse CD19 (PE-Cy7)	BD PharMingen	Cat# 552854; RRID:AB_394495
Rat Anti-mouse IgM (FITC)	BD PharMingen	Cat# 553437; RRID:AB_394857
Rat Anti-mouse IgG1 (APC)	BD PharMingen	Cat# 550874; RRID:AB_398470
Rat Anti-mouse CD8a (BV650)	Biolegend	Cat# 100742; RRID:AB_2563056
Rat Anti-mouse CD4 (PE)	Biolegend	Cat# 100408; RRID:AB_312693
Rat Anti-mouse CD3 (Alexa Fluor 700)	Biolegend	Cat# 100216; RRID:AB_493697
Rat Anti-mouse CD62L (BV421)	Biolegend	Cat# 104436; RRID:AB_2562560
Rat Anti-mouse CD44 (BV711)	Biolegend	Cat# 103057; RRID:AB_2564214
Rat Anti-mouse CD138 (PE)	BD PharMingen	Cat# 553714; RRID:AB_395000
Rat Anti-mouse CD138 (BV650)	BD PharMingen	Cat# 564068; RRID:AB_2738574
Armenian Hamster Anti-mouse CD11c (BV510)	Biolegend	Cat# 117338; RRID:AB_2562016
Rat Anti-mouse CD11b (Alexa Fluor 594)	Biolegend	Cat# 101254; RRID:AB_2563231
Rat Anti-mouse Ly-6G/Ly-6C (Gr-1) (APC/Cyanine7)	Biolegend	Cat# 108424; RRID:AB_2137485
HRP Goat Anti-mouse IgM-HRP	Southern Biotech	Cat# 1021-05; RRID:AB_2794240
HRP Goat Anti-mouse IgG-HRP	Southern Biotech	Cat# 1030-05; RRID:AB_2619742
Unlabelled Goat Anti-mouse IgM	Southern Biotech	Cat# 1020-01; RRID:AB_2794197
Unlabelled Goat Anti-mouse IgG1	Southern Biotech	Cat# 1070-01; RRID:AB_2794408
BRD4 Antibody	Bethyl Laboratories	A301-985A50; RRID:AB_2631450
c-Myc (D84C12) Rabbit mAb	Cell Signaling Technology	Cat# 5605; RRID:AB_1903938
Rabbit (DA1E) mAb IgG Isotype Control	Cell Signaling Technology	Cat# 3900; RRID:AB_1550038
Goat Anti-Rabbit IgG (H&L) Alexa Fluor 647	Thermofisher	Cat# A27040; RRID:AB_2536101
Chemicals, Peptides, and Recombinant Proteins		
JQ1	MedChemExpress	Cat# HY-13030
CTX-0391034	This paper	N/A
Lipopolysaccharides *Escherichia coli* O26:B6	Sigma Aldrich	Cat# L2654
ABTS (2,2-Azino-bis [3-ethylbenzthiazoline-6-sulfonic Acid]	Sigma Aldrich	Cat# A9941
Critical Commercial Assays		
Click-iT RNA Alexa Fluo 594 Imaging Kit	Thermofisher	Cat# C10330
B cell isolation Kit	Miltenyi Biotec	Cat# 130-090-862
CellTrace Violet	Invitrogen	Cat# 34557
RNeasy Mini Kit	QIAGEN	Cat# 74106
RNase-Free DNase Set	QIAGEN	Cat# 79256
QuantSeq 3′ mRNA-Seq Library Prep Kit	Lexogen	NA
ChIP DNA Clean and Concentrator	Zymo Research	Cat# D5201
NEBNext Ultra II DNA Library Prep Kit for Illumina	NEB	Cat# E7645L
Deposited Data		
Raw RNA-sequencing and ChIP-Sequencing Data	This paper	GEO: GSE156126
Experimental Models: Organisms/Strains		
Mouse: C57BL/6J	The Jackson Laboratory	JAX 000664
Mouse: *Bim* KO mice	Bouillet et al. (1999)	NA

(*Continued on next page*)

Continued

REAGENT or RESOURCE	SOURCE	IDENTIFIER
Mouse: *Puma* KO mice	Villunger et al., 2003	NA
Mouse: *Noxa* KO mice	Villunger et al., 2003	NA
Mice: MRL/MpJ-Faslpr/J (MRL-lpr)	The Jackson Laboratory	JAX 000485
Oligonucleotides		
CpG 1668	Geneworks	5′-3′ TCCATGACGTTCCTGATGCT
Software and Algorithms		
Cutadapt v1.9	Martin, 2011	https://journal.embnet.org/index.php/embnetjournal/article/view/200
HISAT2	Kim et al., 2019	https://idp.nature.com/authorize?response_type=cookie&client_id=grover&redirect_uri=https%3A%2F%2Fwww.nature.com%2Farticles%2Fs41587-019-0201-4
Bowtie (v2.2.3)	Langmead and Salzberg, 2012	http://bowtie-bio.sourceforge.net/bowtie2/index.shtml
Samtools (v1.3)	Li et al., 2009	https://github.com/samtools/samtools
FeatureCounts	Liao et al. (2014)	https://www.ncbi.nlm.nih.gov/pubmed/24227677
Voom-LIMMA packages	Law et al. (2014)	https://genomebiology.biomedcentral.com/articles/10.1186/gb-2014-15-2-r29
IGVTools (V2.3.72)	Broad Institute	https://software.broadinstitute.org/software/igv/download
MACS2 (V2.0.10)	Zhang et al., 2008	https://github.com/macs3-project/MACS/
IGV (V2.3.55)	Broad Institute	https://software.broadinstitute.org/software/igv/download
HOMER (v4.8.3)	Heinz et al., 2010	http://homer.ucsd.edu/homer/
Csaw	Lun and Smyth, 2016	https://www.bioconductor.org/packages/release/bioc/html/csaw.html
Coltron (v1.0.2)	NA	https://pypi.org/project/coltron/
ROSE2 (v1.0.5)	NA	https://pypi.org/project/rose2/1.0.5/
GSEA2-2.2.2	Subramanian et al. (2005); Mootha et al., 2003	https://www.gsea-msigdb.org/gsea/index.jsp
Other		
Dynabeads Protein G	Thermofisher	Cat# 10004D
Dynabeads Protein A	Thermofisher	Cat# 10002D

RESOURCE AVAILABILITY

Lead Contact

Further information and requests for resources and reagents should be directed to and will be fulfilled by the Lead Contact, Edwin Hawkins (hawkins.e@wehi.edu.au).

Materials Availability

There are restrictions to the availability of CTX-0391034 due to the limited quantity of the material remaining. However, full details of the synthetic route to make CTX-0391034 has been provided in the Method Details section to enable the independent synthesis of this compound.

Data and Code Availability

The datasets generated during this study are available at GEO: GSE156126.

EXPERIMENTAL MODEL AND SUBJECT DETAILS

Male and female C57BL/6 of 8-12 weeks and B6.MRL/lpr mice of 5-27 weeks of age were used for experiments. Mice deficient of Bim, Noxa and Puma were kindly provided by Phillipe Bouillet (The Walter and Eliza Hall Institute (WEHI), Parkville, Victoria, Australia).

All mice were bred and maintained under specific pathogen-free conditions in the WEHI animal facility (Kew, Victoria, Australia). Mice were maintained in specific pathogen-free conditions at the WEHI animal facilities (Parkville, Victoria, Australia) and all experiments performed in accordance with WEHI animal ethics committee regulations.

METHOD DETAILS

Cell culture

Cell cultures were performed as previously described (Hawkins et al., 2013b; Waibel et al., 2018). Briefly, naive B cells were purified using a discontinuous Percoll (GE Healthcare) gradient and a B cell isolation kit (Cat# 130-090-862 Miltenyi Biotec). Purity of the B cell population was verified as > 95% $B220^+$ $CD19^+$ by flow cytometry. B cells were stimulated with lipopolysaccharide derived from *Escherichia coli 026:B6* (LPS; 15 μg/mL; Cat#L2654, Sigma) or CpG (3 μM; Geneworks), with the addition of specified concentration of JQ1. To track proliferation of the cells, B cells were labeled with CellTrace Violet (CTV; Cat#34557, Invitrogen) as per manufacturer's protocol.

Quantitative analysis

Absolute cell number was determined with addition of $1x10^4$ calibration beads directly to cells prior to analysis. 0.2μM Propidium iodide (PI) was also added with the beads to identify dead cells by exclusion. Ratio of live cells to beads was measured by flow-cytometry to determine the absolute live cell number in culture. Cohort analysis was performed as described by Hawkins et al. (2007a) For *in vitro* differentiation studies, B cells were stained using CD138 (clone 281-2, Cat#564068, BD PharMingen).

In vitro drug preparation

JQ1 (a kind gift from Prof. Ricky Johnstone – Peter MacCallum Cancer Centre, Parkville, Victoria, Australia) and PRMT5 inhibitor (see the synthesis of CTX-0391034 section below) were diluted in dimethyl sulfoxide (DMSO) and used at concentrations indicated in figures.

Intracellular staining of Myc

Intracellular staining of Myc was performed as previously described (Liao et al., 2014). Briefly, cells were harvested at the time points indicated and were immediately resuspended in fixation buffer (0.5% paraformaldehyde, 0.2% Tween-20 and 0.1% bovine serum albumin in PBS) at room temperature, for at least 24 hours until staining was performed. Fixed cells were stained with either anti-Myc (clone D84C12, Cell Signaling Technology) or a rabbit IgG isotype-matched control antibody (clone D1AE, Cell Signaling Technology) before staining with an anti-rabbit IgG conjugated to Alexa Fluor 647. Staining of all fixed samples within one experiment was performed at the same time.

Intracellular staining of nascent RNA

5-ethynyl uridine (EU) (Click-iT RNA Alexa Fluor 594 Imaging Kit, Cat# C10330, Thermofisher Scientific) was added (500uM final) to cultured cells at specified time point and incubated under normal cell culture conditions for 1 hour. Cells were harvested and were immediately resuspended in fixation buffer (0.5% paraformaldehyde, 0.2% Tween-20 and 0.1% bovine serum albumin in PBS) at room temperature, for at least 24 hours until staining was performed. Fixative was removed and cells were washed with PBS twice prior to staining with 100uL cocktail mix from the kit (85.6uL Reaction buffer, 4uL $CuSO_4$, 0.125uL AF549 and 10.3uL 1X Buffer Additive) per sample. Cells were stained for 30 minutes at room temperature away from light. Stained cells were washed with Rinse buffer, followed by PBS and lastly washed twice with fixation buffer. Myc staining was performed as described above following the wash step.

ELISA assays

Supernatant was removed from lymphocyte cultures and stored at −20°C until ELISA analysis. All antibodies were purchased from Southern Biotechnology Associates. 96-well ELISA plates (Cat#CLS3795, Sigma-Aldrich) were coated with either goat anti-mouse IgM (1.20-01; 1:500) or IgG1 (1070-01; 1:500), washed and exposed to a titration of supernatant samples. Plates were washed and the bound Ig was detected using horseradish peroxidase conjugated goat anti-mouse IgM (1020-05; 1:1000) or IgG1 (1070-05; 1:2000). Plates were visualized with the addition of ABTS (2,2-Azino-bis [3-ethylbenzthiazoline-6-sulfonic Acid]; Sigma-Aldrich). Purified Ig isotype standards (Sigma-Aldrich) were used to determine the serum Ig concentrations. Color development was analyzed on VersaMax ELISA microplate reader (Molecular Devices), using wavelengths 415 minus 492.

RNA sequencing and analysis

Total RNA was extracted using RNeasy® Mini Kit (QIAGEN, Hilden, Germany). The extracted RNA was analyzed on the Agilent 4200 Tapestation prior to library preparation. High quality RNA with RIN values greater than 9 was used for downstream application. 3′mRNA-sequencing libraries were prepared from 100ng of total RNA using the QuantSeq 3′ mRNA-Seq Library Prep Kit (Lexogen) according to the manufacturers instructions and sequenced on the NextSeq 500 (Illumina). The single-end 75bp were demultiplexed using CASAVAv1.8.2 and Cutadapt (v1.9) was used for read trimming. The trimmed reads were subsequently mapped to the mouse

genome (mm10) using HISAT2. FeatureCounts was used for read counting (Law et al., 2014) after which differential gene expression analysis was performed using Voom-LIMMA packages (Liberzon et al., 2015). GSEA2-2.2.2 was used for Gene set enrichment analysis (GSEA) (Subramanian et al., 2005; Waibel et al., 2015).

ChIP-Sequencing and analysis

B cells were cross-linked with 2% formaldehyde for 10 minutes at room temperature and quenched with addition of 1.25M glycine. Cells were washed twice (5% BSA, 800 g, 5min, 4C) and lysed in nuclear extraction buffer (20mM Tris, pH 8.0, 10mM NaCl, 2mM EDTA, pH 8.l0, 0.5% Igepal CA-630 and 1x Complete Protease Inhibitor (Roche)) three times. Nuclei resuspended in sonication buffer (20mM Tris pH 7.5, 150 mM NaCl, 2 mM EDTA, 1% Igepal CA-630, 0.3% sodium dodecyl sulfate and 1 × Complete protease inhibitor (Roche)) and sonicated with a Covaris S220 sonicator (peak power, 105; duty factor, 20; cycle/burst, 200; duration, 750 s). Samples were cleared by centrifugation at 12,000 g for 20 min, and one volume of dilution buffer (20 mM Tris-HCl, pH 8.0, 150 mM NaCl, 2 mM EDTA, 1% Triton X-100 and 1 × Complete protease inhibitor (Roche)) was added to cleared chromatin. Samples were precleared with 20 μl Dynabeads Protein G (Life Technologies) blocked with 0.1% BSA for 2 h. BSA was added to precleared chromatin to a final concentration of 0.1%. 1% chromatin was taken as input. Immunoprecipitation was performed overnight at 4°C with rotation with 2 μg antibody (Bethyl A301-985A100). Immunoprecipitated samples were captured by incubation with 20 μl Dynabeads Protein G (Life Technologies) blocked with 0.1% BSA for 2 h. Beads were then washed twice each with wash buffer 1 (20 mM Tris, pH 8.0, 150 mM NaCl, 2 mM EDTA, 1% Triton X-100 and 0.15% SDS), wash buffer 2 (20 mM Tris, pH 8.0, 500 mM NaCl, 2 mM EDTA, 1% Triton X-100 and 0.1% SDS), wash buffer 3 (20 mM Tris, pH 8.0, 250 mM LiCl, 2 mM EDTA, 0.5% Igepal CA-630 and 0.5% sodium deoxycholate) and TE buffer (10 mM Tris, pH 7.5, 1 mM EDTA). DNA was eluted with 100uL elution buffer (0.1M NaHCO3, 1% SDS) for 30 minutes twice and reverse crosslinked. DNA product was purified using Zymo ChIP DNA Clean and Concentrator Kit. ChIP-enriched DNA was processed and sequenced using NEBnext Ultra II kit according to manufacturer's instructions on Nextseq500 (Illumina). 20 million single-end 75bp reads were generated per sample. CASAVA (v1.8.2) was used for demultiplexing. The FASTQ files generated were aligned to the mouse reference genome (mm10) using bowtie (v2.2.3). Samtools (v1.3) was used for manipulation of SAM and BAM files and MACS (V2.0.10) was used for peak calling. TDF files were generated using IGVTools (V2.3.72) and ChIP-Seq tracks were visualized using IGV (v2.3.55). HOMER (v4.8.3) was used for quantification and annotation of the ChIP-Seq datasets after which R was used for visualization. Quantification of Brd4 displacement and statistical analysis of ChIP-Seq datasets were performed using csaw (Lun and Smyth, 2016).

Super enhancer analysis

Samtools (v1.9) was used for the removal of potential PCR duplicates and indexing of BAM files. MACS (v2.1.1) was used for narrow peak calling with default parameters. BED files generated were filtered with Bedtools (v2.27.1) to remove peaks that fall into ENCODE mm10 blacklist regions and transformed into GFF file format using Rstudio (v3.6.1) to meet the input criteria for ROSE2 (v1.0.5). Superenhancers were identified with the ROSE2 (v1.0.5) algorithm with a stitching distance of 12.5Kb and a TSS exclusion zone of 2Kb. Transcription factor networks were constructed with the Coltron (v1.0.2) algorithm where only H3K27ac ChIP-seq signal and a ROSE2 generated enhancer table were provided as input. Remaining parameters were left as default.

In vivo JQ1 therapy

B6.MRL/lpr mice were dosed via intraperitoneal injection once daily for a period of 28 days (5 days on, 2 days off). Vehicle groups received 10% w/v 2-hydroxypropyl-beta-cyclodextrin (HPBCD) (Sigma) in MilliQ water (Millipore Corporation). JQ1 was diluted in 10% w/v HPBCD to 5mg/mL and administered to mice at 25mg/kg. 100 μL of blood was extracted from each mouse via mandible or retro-orbital sinus bleed at 14-day intervals. At end point, mice were euthanized. Blood was extracted via cardiac bleed, while spleens and bone marrow were isolated for flow cytometry analysis. Red blood cells were lysed and immune subsets quantified by antibody staining against CD4, CD8, CD3, CD62L, CD44, B220, CD19, CD138, CD11c, CD11b, Gr-1. Total cell numbers were determined by reference to a known number of calibration beads as previously described (Waibel et al., 2015). Serum for antinuclear antibody analysis was incubated with nuclear extract (E589B) coated plates, and murine antibodies detected using goat anti-mouse IgM and IgG HRPO (Southern Biotech).

Synthesis of CTX-0391034

(*S*)-*N*-(3-(3,4-Dihydroisoquinolin-2(*1H*)-yl)-2-hydroxypropyl)-4-(morpholine-4-carbonyl)benzamide (Figure S8A).

A solution of 4-(4-morpholinylcarbonyl)benzoic acid (1.30 g, 5.53 mmol) in MeCN (15 mL) was cooled to 0°C. HATU (3.15 g, 8.29 mmol) was added followed by a solution of (*S*)-1-amino-3-(3,4-dihydroisoquinolin-2(1*H*)-yl)propan-2-ol (1.37 g, 6.63 mmol,) in MeCN (50 mL) and DIPEA (2.89 mL, 16.6 mmol). The reaction was stirred at 0°C for 2 hours. The mixture was quenched with 5% w/v aqueous sodium carbonate (50 mL) and the organic solvents removed *in vacuo*. The aqueous residue was extracted with EtOAc (3 × 50 mL) and the pooled organic extracts were washed with water (50 mL) and brine (50 mL), dried over magnesium sulfate, filtered and concentrated. The resultant mixture was purified by column chromatography (40 g SiO_2 cartridge, 50%–100% EtOAc (with 1% v/v of a 2.0 M NH_3 in MeOH solution) in petroleum benzine 40-60°C followed by 0%–20% MeOH in EtOAc (with 1% v/v of a 2.0 M NH_3 in MeOH solution)). Collection of the suspected product fractions followed by removal of the solvent *in vacuo* gave pale yellow oil. The oil was purified by SCX cartridge (10 g, 3 column volumes of MeOH followed by 3 column volumes of

0.2 M methanolic ammonia) and the basic filtrate was dried *in vacuo* to give yellow oil. The oil was purified by column chromatography (40 g SiO_2 cartridge, 0%–15% MeOH in EtOAc (modified with 1% v/v of a 2.0 M NH_3 in MeOH solution)) and the product was precipitated by sonication in diethyl ether followed by removal of the solvent *in vacuo* (4 repeats) to give the title compound (1.088 g, 46% yield, purity 98%) as a white solid. ^{1}H NMR (400 MHz, d_4-Methanol): δ 7.88 – 7.82 (m, 2H), 7.45 – 7.40 (m, 2H), 7.16 – 7.07 (m, 3H), 7.06 – 7.00 (m, 1H), 4.17 – 4.06 (m, 1H), 3.76 (s, 6H), 3.67 – 3.36 (m, 6H), 2.95 – 2.85 (m, 4H), 2.76 – 2.62 (m, 2H); ^{13}C NMR (101 MHz, d_6-DMSO): δ 168.50, 165.76, 138.01, 135.43, 134.97, 134.15, 128.45, 127.35, 126.91, 126.42, 125.99, 125.49, 66.77, 66.08, 62.56, 56.12, 51.26, 45.01, 28.73; LCMS-B: RT 3.10 min; (m/z) 424 $[M+H]^+$; HRMS (m/z): $[M]^+$ cacld. for C_{24} H_{29} N_3 O_4, 423.2158; found 423.2173. (Figures S8B and S8C)

QUANTIFICATION AND STATISTICAL ANALYSIS

Significance was calculated for *in vitro* and *in vivo* experiments as specified in figure legends using either ANOVA or two-tailed unpaired Student's t tests, assuming Gaussian distribution and equal standard deviations between experimental and control groups. Differences were considered statistically significant where p value < 0.05. n represents number of animals.